RSC Advances

PAPER

View Article Online
View Journal | View Issue

Cite this: *RSC Adv.*, 2025, **15**, 19392

Encapsulation of progesterone in reishi mushroom composite for optimized hormone replacement and targeted anticancer therapy

Samar M. Mahgoub,[a] Abdullah S. Alawam,[b] Hassan A. Rudayni,[b] Ahmed A. Allam,[b] Aya Shaban,[c] Esraa Khaled,[d] Aya M. Mokhtar,[e] Sahar Abdel Aleem Abdel Aziz[f] and Rehab Mahmoud *[g]

Conventional hormone replacement therapy (HRT) and hormone-dependent cancer treatments face significant challenges, including poor bioavailability, rapid metabolism, and adverse side effects of progesterone, as well as limited targeting efficiency and systemic toxicity. To address these issues, this study develops an innovative progesterone–reishi mushroom (*Ganoderma lucidum*) composite, leveraging the natural bioactive properties of reishi mushrooms to enhance therapeutic efficacy. The composite was prepared by encapsulating progesterone within the reishi mushroom matrix, achieving a high loading efficiency of 98.10%. Characterization using FTIR, SEM, XRD, and UV-Vis confirmed successful encapsulation and interaction between progesterone and the mushroom matrix. *In vitro* release studies demonstrated a sustained and controlled release profile, with 88.25% of progesterone released over 48 hours, compared to the rapid and complete release of free progesterone within 2–4 hours. Kinetic modeling revealed a non-Fickian diffusion mechanism, indicating a synergistic interaction between the hormone and the mushroom matrix. *In vitro* cytotoxicity assays on MCF-7 breast cancer cells showed that the composite exhibited enhanced anticancer activity, with an IC_{50} of 81.11 μg mL^{-1}, significantly lower than free progesterone (IC_{50} = 123.12 μg mL^{-1}). Molecular docking studies highlighted the strong binding affinities of ganoderic acid A (a bioactive compound from reishi mushrooms) and progesterone with key receptors (PCL-2, PI3K, PR, ERα), suggesting potential synergistic effects in hormone regulation and cancer inhibition. Antimicrobial assays revealed the composite's potent activity against Gram-positive pathogens, such as *Streptococcus agalactiae* (MIC = 41.60 μg mL^{-1}) and *Staphylococcus aureus* (MIC = 52.10 μg mL^{-1}), with bactericidal effects (MBC/MIC < 4). Accelerated stability testing (40 ± 2 °C/75 ± 5% RH, 6 months) showed >94% progesterone retention, sustained release, stable colloidal properties, and minimal loss of antimicrobial activity against bacteria and *Candida albicans*, confirming its stability and efficacy. This research demonstrates the promise of combining natural bioactive compounds with synthetic hormones for targeted, effective therapies. The progesterone–reishi mushroom composite offers a dual-action approach, integrating hormonal regulation with anticancer and antimicrobial properties, paving the way for novel treatments in women's health and cancer therapy.

Received 5th April 2025
Accepted 29th May 2025

DOI: 10.1039/d5ra02368h

rsc.li/rsc-advances

1. Introduction

Hormone replacement therapy (HRT) is a widely used treatment for managing menopausal symptoms, including hot flushes, osteoporosis, and mood disorders.[1] Progesterone, a key hormone in HRT, plays a critical role in regulating the menstrual cycle and maintaining pregnancy.[2] However, conventional progesterone therapies often suffer from poor

[a]*Materials Science and Nanotechnology Department, Faculty of Postgraduate Studies for Advanced Sciences, Beni-Suef University, Egypt. E-mail: miramar15@yahoo.com*

[b]*Department of Biology, College of Science, Imam Mohammad Ibn Saud Islamic University (IMSIU), Riyadh, 11623, Saudi Arabia. E-mail: asalawam@imamu.edu.sa; HARUDAYNI@imamu.edu.sa; aallam@imamu.edu.sa*

[c]*Faculty of Pharmacy, Cairo University, Egypt. E-mail: ayaelhuseani@gmail.com*

[d]*Biotechnology Department, Faculty of Post-Graduate Studies for Advanced Sciences, Beni-Suef University, Beni-Suef, Egypt. E-mail: esraakhaledmahmoud10_pg@psas.bsu.edu.eg*

[e]*Hydrogeology and Environment Department, Faculty of Earth Sciences, Beni-Suef University, Beni-Suef, 62511, Egypt. E-mail: aya2451999mo@gmail.com*

[f]*Department of Hygiene, Zoonoses and Epidemiology, Faculty of Veterinary Medicine, Beni-Suef University, Beni-Suef, 62511, Egypt. E-mail: abdelaziz.sahar@yahoo.com*

[g]*Chemistry Department, Faculty of Science, Beni-Suef University, Beni-Suef, 62511, Egypt. E-mail: rehabkhaled@science.bsu.edu.eg*

bioavailability, rapid metabolism, and undesirable side effects such as weight gain, bloating, and increased risk of cardiovascular events.[3,4] These limitations underscore the need for innovative delivery systems that can enhance progesterone's therapeutic efficacy while minimizing its adverse effects. Similarly, hormone-dependent cancers, such as breast cancer, represent a significant global health burden.[5] Progesterone has shown promise in modulating hormone receptors and inhibiting tumor growth in certain cancers.[6,7] However, its clinical application is limited by systemic toxicity and poor targeting efficiency. Natural bioactive compounds, particularly those derived from medicinal mushrooms, have gained attention for their anticancer, immunomodulatory, and anti-inflammatory properties.[8] Among these, the reishi mushroom (*Ganoderma lucidum*) stands out for its rich composition of triterpenoids, polysaccharides, and other bioactive molecules that exhibit potent anticancer and hormone-regulating effects.[9,10] Despite these benefits, the therapeutic potential of reishi mushrooms is often constrained by poor solubility and bioavailability,[11] highlighting the need for innovative formulations to harness their full potential. The integration of natural bioactive compounds with synthetic or semi-synthetic drugs, such as progesterone, offers a promising strategy to address these challenges. Encapsulation of bioactive compounds within natural matrices, such as the fruiting body of reishi mushrooms, can enhance their stability, bioavailability, and targeted delivery.[12] Moreover, the synergistic effects of progesterone and reishi mushrooms could provide a dual-action therapeutic approach, combining the hormonal regulation of progesterone with the immunomodulatory and anticancer properties of reishi mushrooms. This study aims to develop an innovative encapsulated formulation of progesterone within the fruiting body of reishi mushrooms, leveraging the natural bioactive properties of the mushroom to enhance progesterone's therapeutic efficacy. The resulting composite is expected to address the limitations of conventional HRT and hormone-dependent cancer therapies by providing a safe, natural, and effective delivery system. By combining the unique properties of progesterone and reishi mushrooms, this research seeks to pave the way for novel therapeutic solutions in women's health and cancer treatment. In addition to pharmacological evaluation, the formulation's stability was assessed through an accelerated stability study under ICH Q1A(R2) guidelines to predict shelf-life and ensure functional performance during storage.

2. Experimental section

2.1 Materials and reagents

Progesterone (with purity 99.87%) was purchased from Hubei Gedian Humanwell Pharmaceutical Co., Ltd (E-zhou City, Hubei, China), edible Reishi mushrooms (*Ganoderma lucidum*) were obtained from Xi'an Lesen Bio-Tech Co., Ltd (Xi'an, Shaanxi, China). Ethanol, sodium chloride (NaCl), sodium phosphate dibasic (Na_2HPO_4), potassium phosphate monobasic (KH_2PO_4), and potassium chloride (KCl), sodium hydroxide and hydrochloric acid 37%, all of analytical grade were purchased from Merck (Darmstadt, Germany). Bi-distilled water.

2.2 Preparation of reishi mushroom fruiting body matrix

All *Ganoderma lucidum* (Reishi mushroom) fruiting bodies used in this study were sourced from a single commercial batch (Xi'an Lesen Bio-Tech Co., Ltd, Xi'an, Shaanxi, China) to minimize batch-to-batch variability and ensure consistency throughout the experimental procedures. Upon receipt, the mushrooms were visually inspected for uniformity in color, size, and absence of visible contamination or spoilage. Clean the mushrooms to remove any dirt and debris, then dry the fruiting bodies in a drying oven at 40 °C for 24 hours. For sample preparation, 100 g of fresh Reishi mushroom (*Ganoderma lucidum*) fruiting bodies were used. After drying, the final weight of the dried mushroom was approximately 10 g, corresponding to a moisture loss of about 90%. Once dried, grind the fruiting bodies into a fine powder using a mechanical methods using a Mill (PM 100, Haan, Germany) then sieve the powder in a 100-mesh sieve to achieve a uniform particle size, ensuring consistency for loading. The entire process, from sourcing to powder preparation, was carefully documented for traceability and reproducibility. Analytical characterization of the mushroom matrix, both before and after progesterone loading, was performed using FTIR, SEM, XRD, and UV-Vis spectroscopy to confirm material consistency and successful encapsulation.

2.3 Loading progesterone into the mushroom matrix

The loading of progesterone into the reishi mushroom matrix powder involves a 10 : 1 w/w ratio of mushroom powder to progesterone, which is mechanically mixed and embedded using a Planetary Ball Mill (PM 100, Haan, Germany) at 300 rpm for 60 minutes. This process ensures thorough integration of progesterone into the porous structure of the mushroom matrix, facilitated by mechanical forces that break down particles and promote uniform distribution.[13–15] The resulting mixture is sieved through a 100-mesh sieve to achieve a uniform particle size, ensuring consistency for further use.[16] Interactions between progesterone and the reishi matrix include physical embedding and adsorption due to the mushroom's porous structure,[17,18] as well as chemical interactions such as hydrogen bonding between progesterone's carbonyl/hydroxyl groups and the functional groups of reishi polysaccharides,[19] hydrophobic interactions with non-polar components like triterpenes,[20] and weak van der Waals forces.[21] These interactions may enhance progesterone's stability, bioavailability, and potential synergistic effects with reishi's bioactive compounds, such as beta-glucans and triterpenes, which could complement its pharmacological properties.[22] Further characterization would provide deeper insights into these interactions, as illustrated in Scheme 1.

2.3 Characterization of the tested compounds

Several analytical techniques were employed to characterize the prepared adsorbents and the formed composites including Fourier Transform Infrared Spectroscopy (FTIR) that was conducted using a Bruker-Vertex 70 instrument *via* the KBr pellet technique, covering 400 to 4000 cm^{-1}. Also, Scanning Electron

Scheme 1 Schematic representation of the experimental workflow for the preparation of the reishi mushroom fruiting body matrix and the loading of progesterone.

Microscopy (SEM) was examined. An Evolution 350 UV-Vis Spectrophotometer (Thermo Fisher Scientific, Massachusetts, USA) was used to measure the progesterone concentrations. pH was determined with an Adwa–AD1030 automatic surface pH meter. The Zetasizer Ultra (Malvern, USA) was used to determine the size, polydispersity index (PDI), and zeta potential of the loaded and unloaded reishi mushroom. The zeta potential and dynamic light scattering (DLS) techniques provide insight into the particle size distribution, surface charge, PDI, and stability of the encapsulated formulation.

2.5 Progesterone loading efficiency

The concentrations of the samples were determined using a spectrophotometric method, based on a standard calibration curve. To establish the optimal analytical wavelength for the maximum absorbance technique, a stock solution of progesterone was prepared at a concentration of 1 mg mL^{-1} in ethanol. A series of dilutions with varying concentrations were then prepared from this stock solution, also using ethanol. These diluted solutions were scanned across a wavelength range of 200–400 nm using an Evolution 350 UV-Vis Spectrophotometer (Thermo Fisher Scientific, Massachusetts, USA) to quantify the progesterone content. The wavelength of maximum absorbance (λ_{max}) was identified at 240 nm.[23,24] The amount of progesterone loaded is calculated by adding 10 mL of ethanol to the composite in a 1 : 10 (w/v) ratio, then vortex the mixture for 1–2 minutes to ensure thorough mixing, followed by sonication for 15 minutes to enhance extraction efficiency; centrifuge the mixture at 4000 rpm for 10 minutes to separate the supernatant, which is then carefully collected and filtered through a 0.22 μm membrane filter to remove any particulate matter, yielding the extracted progesterone which then measured using the UV spectrophotometer.

The amount of progesterone loaded and loading efficiency were calculated using eqn (1) and (2):

$$\text{Amount of progesterone loaded} = C_t \times V \quad (1)$$

where, C_t: concentration of progesterone in the sample, V: the volume of the supernatant used for extraction.

$$\text{Loading efficiency } (\%) = \frac{\text{amount of progesterone loaded}}{\text{total amount of progesterone used}} \times 100 \quad (2)$$

2.6 *In vitro* release study

The *in vitro* drug release of progesterone encapsulated in the fruiting body of reishi mushroom was evaluated using the dialysis bag method to simulate controlled drug release. Dialysis bags (cellulose membrane, molecular weight cut-off 14 000 Da, SERAVA Electrophoresis) were soaked overnight in the respective release medium prior to use. For each experiment, 50 mg of the encapsulated composite (progesterone-loaded reishi mushroom) and an equivalent amount of free progesterone (as control) were placed in separate dialysis bags, which were sealed at both ends with thermo-resistant thread. These bags were then immersed in 900 mL of either phosphate-buffered saline (PBS, pH 7.4), simulated gastric fluid (SGF, pH 1.2), or simulated intestinal fluid (SIF, pH 6.8) to evaluate the stability and release profile of the composite under different physiological conditions. PBS was prepared by dissolving 8 g NaCl, 0.2 g KCl, 1.44 g Na_2HPO_4, and 0.24 g KH_2PO_4 in approximately 800 mL distilled water, adjusting the pH to 7.4 with 1 M HCl or 1 M NaOH, and making up the volume to 1 L. SGF was prepared by dissolving 2.0 g NaCl and 7.0 mL concentrated HCl in 1 L distilled water and adjusting the pH to

1.2. SIF was prepared by dissolving 6.8 g KH_2PO_4 in 1 L distilled water and adjusting the pH to 6.8 with 0.2 N NaOH. All release studies were conducted at 37 °C ± 0.5 °C in a shaker incubator (Labsol, India) set at 50 rpm. At predetermined time intervals (10 min, 30 min, 1 h, 2 h, 4 h, 6 h, 8 h, 12 h, 24 h, and 48 h), 5 mL aliquots of the release medium were withdrawn and replaced with an equal volume of fresh medium to maintain sink conditions. Each sample was filtered through a 0.22 μm nylon syringe filter to remove any particulate matter. The concentration of progesterone released into the medium was measured using a UV-Vis spectrophotometer at 240 nm. The cumulative drug release percentage was calculated by plotting the concentration of released progesterone against time, allowing for evaluation and comparison of the release profiles of the encapsulated and free progesterone in each medium. Drug release at time t, cumulative drug release (%) were calculated using eqn (3) and (4):

$$\text{Released drug at time } t = C_t \times V \tag{3}$$

$$\text{Cumulative drug release (\%)} = \frac{\text{released drug at time } t}{\text{initial amount of drug loaded}} \times 100 \tag{4}$$

where, C_t represents the drug concentration at time t (mg mL^{-1}), V represents volume of the dissolution medium (mL).

2.7 *In vitro* release kinetics

Various release kinetics models were applied including zero-order kinetics (constant release rate), first-order kinetics (release rate depends on the amount of drug remaining), Korsmeyer–Peppas model (power law), Higuchi model (diffusion-controlled release) to give insight into the release mechanism either through diffusion, swelling, or erosion of the progesterone-loaded reishi mushroom composite using the following equations:

Zero-order kinetics

$$M_t = M_0 + Kt \tag{5}$$

First-order kinetics

$$\frac{M_t}{M_0} = 1 - e^{-k_1 t} \tag{6}$$

Korsmeyer–Peppas model

$$\frac{M_t}{M_0} = Kt^n \tag{7}$$

Higuchi model

$$M_t = K_H \sqrt{t} \tag{8}$$

M_t = amount of drug released at time t, M_0 = initial amount of drug, k_1 = first-order rate constant, n is the release exponent that indicates the release mechanism, t = time, k_H = Higuchi rate constant (depends on properties like the diffusion coefficient, solubility, and surface area).

2.8 *In vitro* cytotoxicity and cell viability

2.8.1 Cell lines and culture conditions. MCF-7 cells, a human breast cancer cell line, were obtained from the American Type Culture Collection (ATCC, Manassas, VA, USA). The cell lines were propagated and tested for cytotoxicity assays at Tissue Culture Unit of the Regional center for Mycology and Biotechnology, Al-Azhar University. These cells were propagated in RPMI-1640 medium (Lonza, Belgium) supplemented with 10% inactivated fetal bovine serum (FBS) and 50 μg mL^{-1} gentamycin (Lonza, Belgium). The cells were maintained at 37 °C in a humidified atmosphere containing 5% CO_2 and were subcultured three times per week.

2.8.2 Cytotoxicity evaluation *via* MTT assay. To evaluate the cytotoxicity of the tested compounds, MCF-7 cells were cultured in Corning® 96-well tissue culture plates at a density of 5×10^4 cells per well and incubated for 24 hours. After this period, the cells were treated with varying concentrations of the compounds in triplicate for an additional 24 hours. Six vehicle controls, consisting of media, were included on each plate. Following the incubation, the media was removed and replaced with 100 μL of fresh RPMI-1640 medium (without phenol red). To assess cell viability, 10 μL of a 12 mM MTT stock solution (5 mg MTT in 1 mL of PBS) was added to each well, and the plates were incubated at 37 °C with 5% CO_2 for 4 hours. After incubation, 85 μL of the medium was removed, and 50 μL of DMSO was added to each well to dissolve the formazan crystals. The plates were then thoroughly mixed and incubated at 37 °C for an additional 10 minutes. The absorbance was measured at 590 nm using a microplate reader (SunRise, TECAN, Inc., USA). Cell viability was calculated as a percentage of the optical density (OD) of treated cells relative to the OD of untreated control cells using the following equation:

$$\text{Percentage of viability (\%)} = \left[\left(\frac{OD_t}{OD_c}\right) \times 100\right] \tag{9}$$

where OD_t is the mean optical density of treated wells and OD_c is the mean optical density of untreated wells. Survival curves were constructed by plotting the percentage of viable cells against the drug concentration. The 50% inhibitory concentration (IC_{50}), defined as the concentration required to inhibit 50% of viable cells, was calculated from the dose–response curve using GraphPad Prism version 9.0 (GraphPad Prism software, San Diego, CA, USA). All experiments were performed in triplicate, and results are expressed as mean ± standard deviation (SD). Statistical analysis of IC_{50} values among different treatment groups (free progesterone, reishi mushroom, and progesterone–reishi mushroom composite) was conducted using one-way analysis of variance (ANOVA) followed by Tukey's post hoc test for multiple comparisons. A p-value < 0.05 was considered statistically significant. All statistical analyses were performed using GraphPad Prism version 9.0.

2.9 Molecular docking study

2.9.1 Molecular docking methodology. Molecular docking studies were performed using PyRx 0.8,[25] a virtual screening tool that integrates AutoDock and AutoDock Vina for predicting

protein–ligand interactions. A blind docking approach was employed to identify potential binding sites across the entire surface of the target proteins. The docking grid was configured to encompass the entire protein structure, with grid box dimensions automatically calculated by PyRx to ensure comprehensive coverage. Docking simulations were executed using the AutoDock Vina algorithm, which employs a stochastic search method to predict optimal ligand binding poses. The exhaustiveness parameter was set to 8 to ensure thorough sampling of the binding space.

2.9.2 Visualization and analysis. The docked complexes were visualized and analyzed using BIOVIA Discovery Studio Visualizer (v24.01.23298).[26] Binding affinities (ΔG values) were assessed, and key intermolecular interactions such as hydrogen bonds and hydrophobic interactions were identified and reported. These analyses provided detailed insights into the ligand–protein binding mechanisms and the potential therapeutic efficacy of the compounds.

2.9.3 Docking simulations overview. Docking simulations were conducted to evaluate the binding affinity of ganoderic acid A, a bioactive triterpenoid from *Ganoderma lucidum* (reishi mushroom),[27] and progesterone, a steroid hormone, with target receptors involved in hormone regulation and cancer progression. The selected receptors including PCL-2, PI3K, progesterone receptor (PR), and estrogen receptor alpha (ERα) were chosen based on their well-established roles in these processes: PCL-2 is involved in progesterone-mediated signaling and metabolic regulation,[28] PI3K plays a central role in cell survival and proliferation and is frequently dysregulated in cancers,[29] PR mediates the physiological effects of progesterone in reproductive health,[30] and ERα drives hormone-dependent cancers such as breast cancer.[31] The selection of ganoderic acid A (GAA) as the ligand was based on its well-established pharmacological relevance. GAA is one of the principal triterpenoids isolated from *Ganoderma lucidum* (reishi mushroom), a medicinal fungus extensively used in traditional Asian medicine.[32,33] Ganoderic acid A has demonstrated a broad spectrum of biological activities, including anticancer, anti-inflammatory, and antioxidant properties.[34–36] Notably, its lanostane-type triterpenoid structure closely resembles that of endogenous steroid hormones such as progesterone, suggesting a potential for interaction with nuclear hormone receptors like the progesterone receptor (PR) and estrogen receptor alpha (ERα). These structural and functional characteristics support its candidacy as a bioactive compound for investigation in the context of hormone replacement therapy (HRT) and hormone-dependent cancers. The selection of PR, ERα, phosphoinositide 3-kinase (PI3K), and B-cell lymphoma 2 (BCL-2) as molecular docking targets was based on their critical roles in hormone signaling (PR and ERα) and oncogenic pathways (PI3K and BCL-2), which are commonly dysregulated in hormone-responsive cancers.[37–39] This combination was intended to explore both the potential endocrine activity and anticancer effects of ganoderic acid A in comparison to natural progesterone.

2.9.4 Ligand preparation. The 3D structures of ganoderic acid A and progesterone were retrieved from the PubChem database in SDF format. Ligand preparation was performed using Chem3D 17.0, which included energy minimization using the MMFF94 force field to optimize the molecular structures for docking.

2.9.5 Protein preparation. The crystal structures of the target proteins including PCL-2 (PDB: 2YV6), PI3K (PDB: 8SC8), progesterone receptor (PR) (PDB: 1A28), and estrogen receptor alpha (ERα) (PDB: 1A52) were retrieved from the RCSB Protein Data Bank. Protein preparation was carried out using AutoDock Tools 1.5.7,[40] which involved: Removing water molecules, adding polar hydrogens, and Assigning Kollman charges to ensure accurate docking simulations.

2.10 Antimicrobial assays

2.10.1 Preparation of the microbial isolates and chemical suspensions. *Escherichia coli* (*E. coli*), *Klebsiella puemoniae* (*K. puemoniae*), *Staphylococcus aureus* (*S. aureus*), and *Streptococcus agalactiae* (*Str. agalactiae*) as well one fungal species, *Candida albicans* (*C. albicans*) was used in this study. All isolates have been recovered from farm animals exhibiting clinical manifestations of mastitis in order to evaluate the antibacterial properties of reishi mushrooms (RM) and the encapsulating formula (HP-RM).[41] Briefly, pure, distinct colonies from each strain of bacteria and *C. albicans* traits were centrifuged in brain heart infusion broth (BHI, Oxoid, Code: CM1136) for five minutes at 11 000 rpm. After removing the supernatant, 5 mL of sterile normal saline was added and the microbial precipitate were kept as stock. A spectrophotometer was then used to adjust the concentration to an optical density of 0.10 at 625 nm to obtain a 0.5 McFarland's standard (10^8 colony forming unit per milliliter (CFU mL^{-1}), for the bacterial species and 1.4×10^6 CFU mL^{-1} for *C. albicans*). Further, concentrations of 1000 μg mL^{-1} from both reishi mushrooms and the encapsulating formula were made by suspending in 10.0% MSDO (Sigma-Aldrich, USA) and sonicating them for five minutes at a high sonicator with a power of 20 kHz (Model: Q700 Sonicator®, Australia).

2.10.2 Agar well diffusion assay. The antibacterial activity of both reishi mushroom and HP-RM was assessed by the well agar diffusion methodology, Mueller–Hinton medium (MHA, Oxoid, Code R01620) was made, autoclaved, cooled down at 40–50 °C, and allowed to solidify in sterile Petri dishes. Subsequently, the surface of the agar was coated with nearly 100 μL of each tested microbial cultivation solution. A sterile cork borer was used to form four holes in each of the agar dish, that measuring 6 mm in diameter. Approximately 50 μL of each of the chemical solutions that were evaluated were also inoculated into their corresponding wells. Following a 24 hour incubation at 37 °C, the dimensions of the zones of inhibition had been determined in triplicates. Furthermore, 10.0% DMSO was employed as a control negative, whilst the commercial antibiotic drug powder of gentamicin (10 mg mL^{-1}) acted as the control positive.

2.10.3 Minimum inhibitory concentrations (MICs). The standard broth macro-dilution method was utilized to investigate the antimicrobial efficiency of reishi mushrooms and HP-RM. MIC was determined in BHI broth using double-dilution method of both compounds in concentrations at starting

point of 1000, 500, 250, 125, 62.5, 31.3, 15.6 and 7.8 μg mL^{-1}. Then standard bacterial or yeast concentrations (0.5 McFarland reaction) were individually inoculated at each dilution followed by incubation at 37 °C for 24 hours. The lowest concentration of the tested chemical suspensions that did not exhibit any noticeable growth in the tubes is known as the MIC threshold. Also, each experiment was carried out in triplicate, and the means (±) have been calculated.[42]

2.10.4 Minimum bactericidal concentration (MBC) and minimum fungicidal concentration (MFC). Aliquots of around 50 μL from each dilution that did not exhibit any obvious microbial growth were streaked on the surface of Brain Heart Infusion plates (BHI, Oxoid, Code: CM1136) and incubated for 24 hours at 37 °C. The MBC or MFC results are achieved when 100.0% of the pathogen population has been eliminated at the lowest concentration of an antimicrobial agent. Additionally, the means (±) have been established for each experiment, which was performed in triplicate.[43] Furthermore, MBC/MIC ratio were evaluated for each microbial species to evaluate the antimicrobial efficacy of the tested chemicals either as bacteriostatic or fungistatic as well as bactericidal or fungicidal ones.[44]

2.11 Statistical analysis

All analytical evaluations were performed in triplicates, and the Student's *t*-test was used for expressing the results as mean (±) standard deviation (SD). At $P < 0.05$, statistical significance was determined.

2.12 Accelerated stability study

To evaluate the long-term stability of the progesterone–reishi mushroom composite, an accelerated stability study was conducted following the ICH Q1A (R2) guidelines.[45,46] This regulatory framework allows the rapid prediction of product stability under elevated temperature and humidity, making it especially beneficial for innovative formulations combining pharmaceutical and natural components.[47,48] Accelerated stability testing provides a time-efficient alternative to real-time studies and is widely adopted during product development and regulatory review.[49] Recent advancements in stability testing protocols have improved prediction accuracy, particularly for biopolymer-based systems and encapsulated drug formulations.[50]

2.12.1 Sample preparation and storage conditions. Freshly prepared progesterone-loaded reishi mushroom composite samples were packaged in nitrogen-flushed aluminum pouches to protect them from moisture and oxygen.[51] These pouches were stored under accelerated conditions (40 ± 2 °C and 75 ± 5% relative humidity) in a validated climatic chamber (Thermolab Scientific Equipments Pvt. Ltd, Maharashtra, India compliant with ICH Q1A(R2) guidelines.[45] Stability analyses were carried out at 0, 3, and 6 months to evaluate changes in physical, chemical, and functional properties over time. Zero-time (0 months) values represent freshly prepared samples.

2.12.2 Analytical evaluations. At each designated time point (0, 3, and 6 months), a set of analytical assessments was performed in triplicate. Physical stability was examined through visual inspection for color change, caking, and odor, along with measurements of particle size and zeta potential using a Malvern Zetasizer Ultra.[52,53] Chemical stability was assessed by quantifying progesterone content through a validated UV-Vis spectrophotometric method at 240 nm.[24] Functional integrity was evaluated *via in vitro* drug release using a dialysis bag method in phosphate-buffered saline (PBS, pH 7.4) at 37 °C over a 48 hour period, with progesterone concentration determined spectrophotometrically.[54,55] Additionally, antimicrobial activity was assessed at the 0, 3 and 6 months marked by determining the minimum inhibitory concentration (MIC) against *Staphylococcus aureus*, *Str. agalactiae*, *E. coli*, *K. pneumoniae* and *C. albicans* using broth microdilution according to CLSI guidelines.[56,57]

3 Results and discussion

3.1 Characterization of the tested compounds

To evaluate the crystalline nature of reishi mushroom (RM) and loaded sample RM/HP, a powdered X-ray diffraction (XRD)

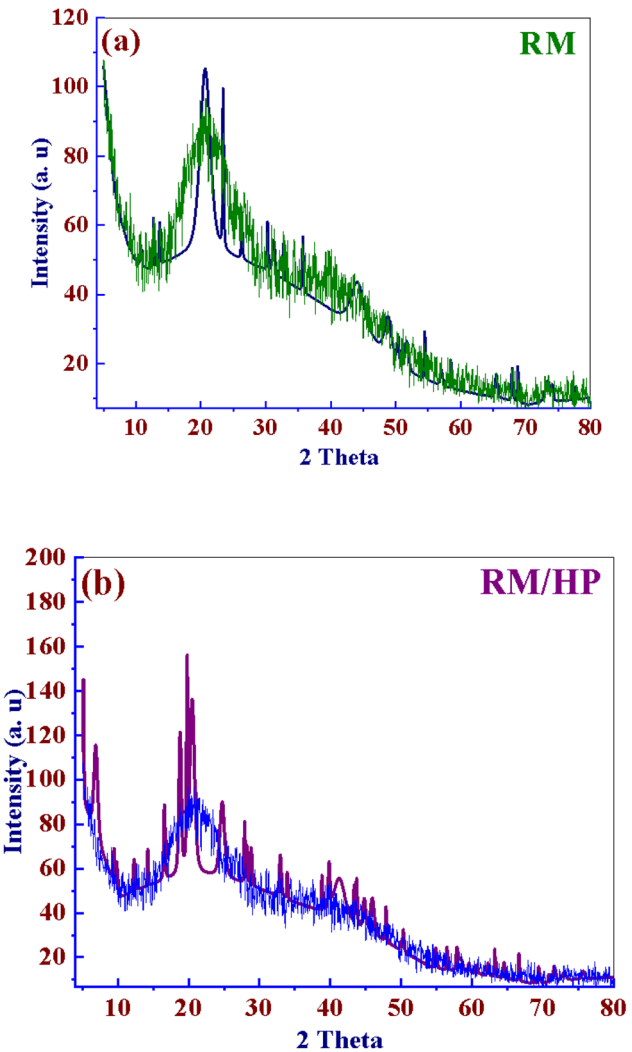

Fig. 1 XRD pattern of (a) RM and (b) after loading RM/HP.

analysis was conducted within the 2θ range of 5° to 80°. The resulting X-ray diffractogram is presented in Fig. 1a and b. The XRD pattern of RM exhibited a broad, hesitant peak at approximately $2\theta = 20.98°$, which indicates the presence of a significant amount of carbon substrate in its composition (Fig. 1a).[58] Notably, the shift towards higher crystallinity in loaded sample which related to that the sample subjected to vibrating and ball milling (Fig. 1b).[59] This enhancement in crystallinity not only validates the efficacy of mechanical processing in disrupting the amorphous matrix of RM walls but also its the potential improvement in the stability and bioavailability of encapsulated HP.[60] Such structural refinements, marked by the modification through the sample crystallinity, elucidate the obvious changes at the molecular level that could augment the functional properties of the RM.[61] Consequently, this detailed exploration of XRD data highlighting the strategic benefits of employing preparation methodologies to optimize the physicochemical attributes and therapeutic efficacy of RM/HP.[62]

Fourier transform infrared (FTIR) spectroscopy was employed to fully characterize the functional groups on the surface of RM in the wavenumber range of 400–4000 cm^{-1}, both before and after loading with progesterone hormone (HP). The results are presented in Fig. 2a–c. A wide band between 3407.39 and 3180.03 cm^{-1} is seen in the powder RM spectra, which is indicative of the vibrational stretching of hydroxyl groups (–OH).[63] Furthermore, the stretching and bending vibrations of saturated C–H bonds are responsible for peaks at 2919 cm^{-1} and 1403.83 cm^{-1}, respectively.[64] The stretching of C=O by amide I is represented by the band at 1642.68 cm^{-1}, whereas the stretching or N–H deformation of amide II contributes to the band at 1560 cm^{-1}. The amide III band at 1250.34 cm^{-1} represents the vibration of the C–N bond.[64,65] Additionally, at 1043.50 cm^{-1} and 1160.05 cm^{-1}, the C–O bond vibrations in alcohol hydroxyl are visible. A notable presence of glucan structure is indicated by the absorption peak at 894 cm^{-1}, which is typical of the β-configuration of D-glucose units.[64,65] One of the most important bands seen in the fingerprint area of D-glucopyranose is the 893 cm^{-1} band, as stated by Barker *et al.*[66] Finally, a saccharide group's bending vibration is represented by the band at 587.96 cm^{-1}.[58] The magnitude of the main peaks rises, and additional peaks appear once HP is loaded onto RM (RM/HP), revealing a relationship between RM and HP. The stretching of the C–H bonds in the CH_2 and CH_3 groups is shown by peaks in the 2919.83–2374.00 cm^{-1} range. Additionally, a peak that corresponds to the stretching of the C=C bond is seen at 1612 cm^{-1}. RM loaded by HP (RM/HP) were studied using FTIR as shown in Fig. 2c. The broad and intense band at 3460.73 cm^{-1} confirms the asymmetric stretching vibration of –OH and N–H groups.[67–69] The strong vibration band at 1642.68 cm^{-1} can be assigned to amide bond (O=C–NH), in consonance with an earlier report.[70] This band could also be assigned to the stretching vibration of C=O and N–H at 1393.16 and 1642.68 cm^{-1} respectively. The small band at 1155.13 cm^{-1} is assigned to C–N.[69] We observed a band observed at 1048.42 cm^{-1} to the C–O stretching.[67,71] Other small bands at 2374.00 cm^{-1} and 2096.58 cm^{-1} could be assigned to the C–N[72] and C≡C[71] stretching vibrations. Also, the reported

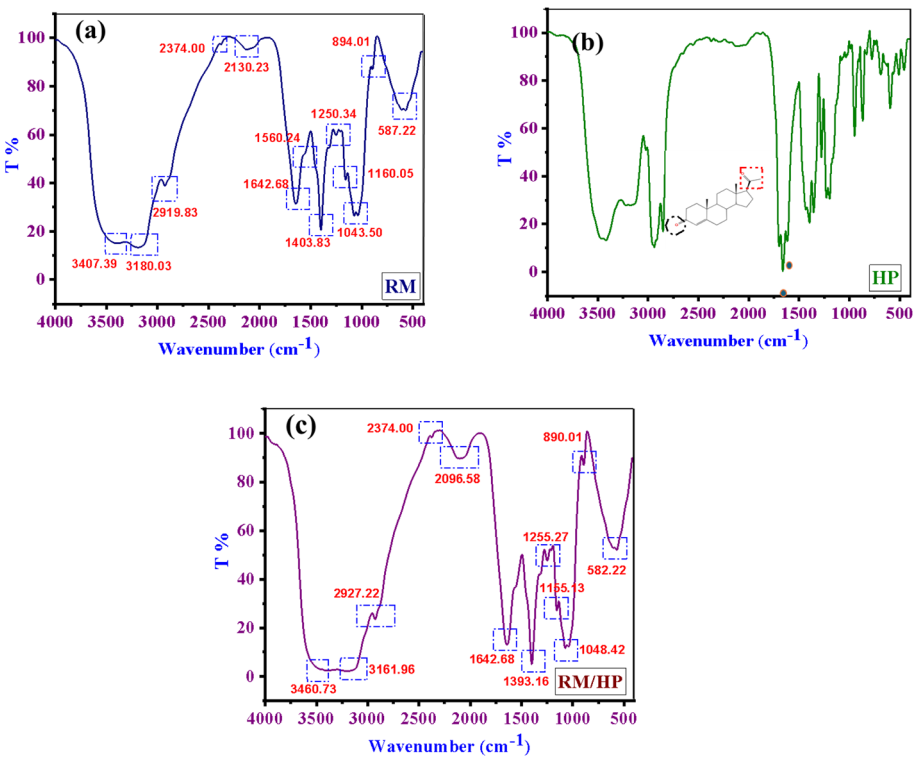

Fig. 2 FTIR spectrum of (a) RM, (b) HP and (c) RM/HP.

the bands between 500 to 900 cm^{-1} in the presented RM spectrum were ascribed to the flavonoid moieties.[68]

HP has characteristic bands located at 1690.50 and 1658.28 cm^{-1} corresponding to the carbonyl groups (C3-cyclic and C20-linked to methyl radical) as shown in Fig. 2b. The characteristic band of the C=C is located between 868.67 and 943.36 cm^{-1}.[73] HP bands regarding to C=O stretching at shifted to 1642.68 cm^{-1} in the loaded sample spectra contacting HP. According to the presence of shifts or changes in the RM/HP spectrum is an indication that they are chemically interacting by chemical bonds like covalent one. In general, one can conclude that all formulations interactions took place between HP and the RM due to the observed changes in the FTIR spectra. The most evident interaction observed in Fig. 2a–c is between HP and RM, due to the increase in the intensity and enlargement of the band located at 1642.68 cm^{-1}. This is in agreement with the results found in the literature.[73] The OH-group, in stretching mode, which confirms the loading of HP molecules in the surface of RM yields a broad peak at 3460.73 cm^{-1} in the RM/HP sample spectra and a sharp peak at 1642.68 cm^{-1}. The broad one may be attributed to the presence of hydrogen bonds on the RM surface. In Fig. 2a and c, the FTIR study evidenced the intramolecular hydrogen bonding among the RM/HP entities. The calculated hydrogen bond intensity was the ratio of the absorbance bands at 3460.73 and 3407.35 cm^{-1} (for the –OH peak) and 1642.68 cm^{-1} (for the bending of C=O peak in two samples) in RM/HP and RM respectively. The absorbance ratio showed an increase in the case of RM/HP loading (0.40) more than that of RM (0.33), indicating the hydrogen bonding interaction between the RM and the loaded HP.

SEM analysis of the resulting powder surface revealed morphological changes in the RM in accordance with the physical modification by mailing (Fig. 3a–c). A significant structural and morphological change resulted by grinding. Following the mailing procedure, the cottony surface was observed, and the loose microstructure was later confirmed by the increased bulk density. The particles were broken up into smaller fractions by extensive milling; the combination of fracture, aggregation, and flattening produced layers of particles. When intermolecular connections are broken, mechanical damage results in a change from an ordered to a disordered (amorphous) structure.[74]

The microstructure of prepared sample after loading reveals that the mycelial fibers are haphazardly wrapped, developed network that is ideal for the creation of porous materials. The SEM micrographs in Fig. 4a–d show layers of irregular RM grows with HP closely and that appeared as a new flower-like morphology with the fibrous one of the materials after loading, attributed to the presence of HP molecules. This structure has high porosity (Fig. 4a), resulting in a significantly higher loading efficiency (98.10%). The network complexation by the functional groups on the HP with the other in the mycelial fibers in RM (image in Fig. 4d). As shown in Fig. 4c, the loaded one has irregular shape, broken structure, rougher surface, denser pores, and loosening in some areas. In addition, the maifanite surface chemically bonded or intercalated with

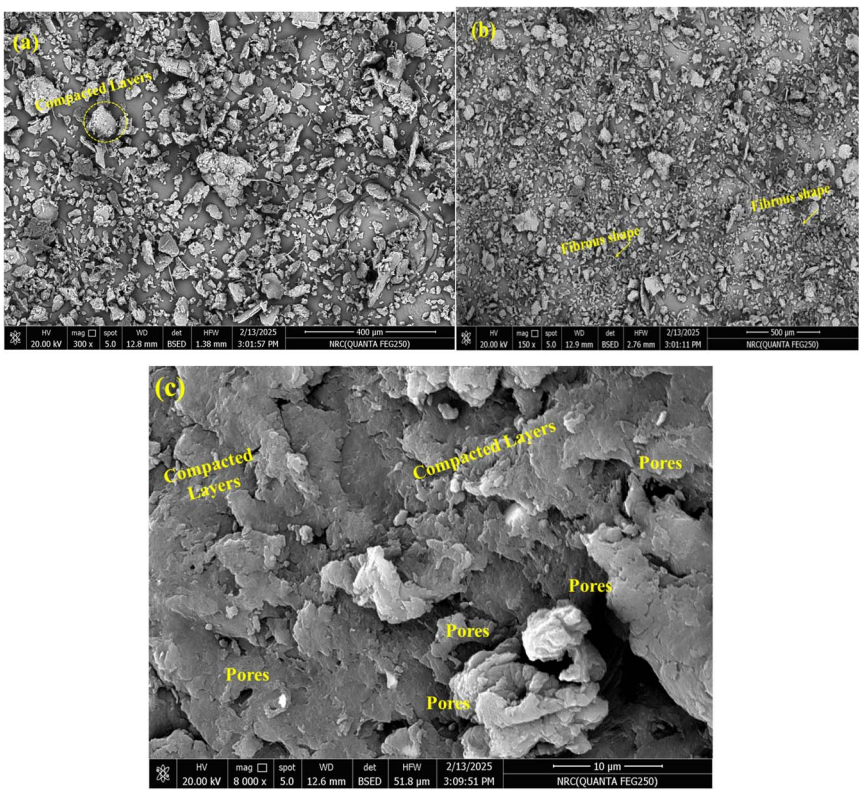

Fig. 3 SEM images of RM.

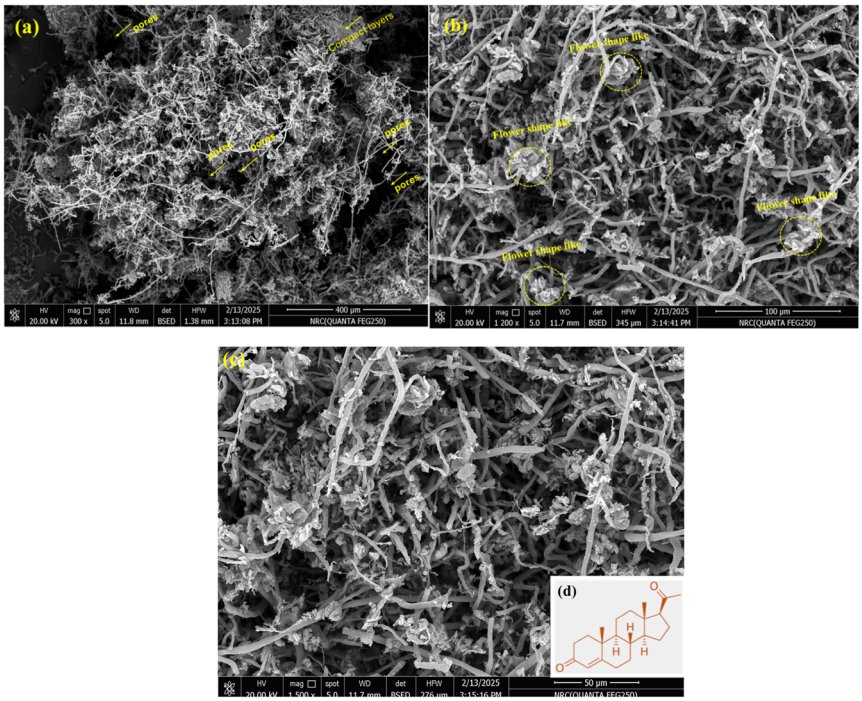

Fig. 4 SEM images of raw RM after hormone loading RM/HP.

HP to form a fibrous structure and flowers stick on the fibers in part of the pores of maifanite. The surface layer of the particle is full of flaky interlayer with more holes and channels.

Surface texture and morphology has gained a lot of interest since it can reveal essential properties, containing heterogeneities and deformations, that might affect the prepared samples utilization. Software called Image J was used to investigate and analysis the geographical SEM image as shown in Fig. 5a–f.[75] The topographical study of RM and RM/HP is shown in Fig. 5a–d, while a cross section of both RM and RM/HP is observed to illustrate the differences. These modifications in texture result in a substantial elevation of surface roughness and waviness, which generates a more varied topographical configuration and an augmentation of the composite's overall porosity and holes. The roughness and waviness of RM (Fig. 5a and c) and RM/HP (Fig. 5b and d) were traced and it was found that the roughness is about small, detailed surface features, while waviness pertains to larger, more pronounced surface variations which is very clear in the loaded material (RM/HP). This improvement is expected to favorably impact both the total surface area and the biochemical interactions of the loaded one (Fig. 5e and f), consequently enhancing its effectiveness for medical applications.

The encapsulated formulation of progesterone exhibits significantly smaller particle size (512.00 ± 2.25 nm) compared to the blank formulation (50.20 ± 1.68 μm), indicating successful nanoscale formulation, which can enhance bioavailability and cellular uptake. The polydispersity index (PDI) decreases from 0.38 to 0.25, suggesting improved uniformity and stability. Additionally, the zeta potential shifts from −33.50 ± 1.21 mV to −42.03 ± 1.63 mV, indicating greater electrostatic repulsion, which enhances colloidal stability and reduces aggregation, as illustrated in Table 1. The formulation also demonstrates high encapsulation efficiency for progesterone (98.10 ± 0.56%), highlighting the efficiency of the encapsulation process that helps to offer enhanced stability, controlled release, and improved therapeutic potential for reishi mushroom.

3.2 *In vitro* release study

The *in vitro* release results demonstrate a clear distinction between the encapsulated progesterone in the reishi mushroom composite and the free progesterone (control), as shown in Fig. 6. Release profiles were evaluated in three physiologically relevant media: simulated gastric fluid (SGF, pH 1.2), simulated intestinal fluid (SIF, pH 6.8), and phosphate-buffered saline (PBS, pH 7.4). In SGF, the composite exhibited a markedly limited release, with less than 20% of progesterone released over 48 hours. This low release is likely due to the acidic environment causing partial denaturation or collapse of the mushroom matrix, as well as reduced solubility of progesterone under such conditions. In SIF, the cumulative release increased to approximately less than 30% over the same period, reflecting a modest improvement but still indicating restricted drug diffusion, possibly due to the mildly basic environment affecting matrix integrity and drug solubility.[76] By contrast, PBS provided an optimal environment for sustained and controlled release. The encapsulated progesterone exhibited an initial burst release of 10.62 ± 1.89% within the first 10 minutes, attributable to surface-bound or loosely entrapped progesterone, followed by a gradual release reaching 88.25 ± 2.33% over 48 hours. This sustained profile is attributed to the reishi

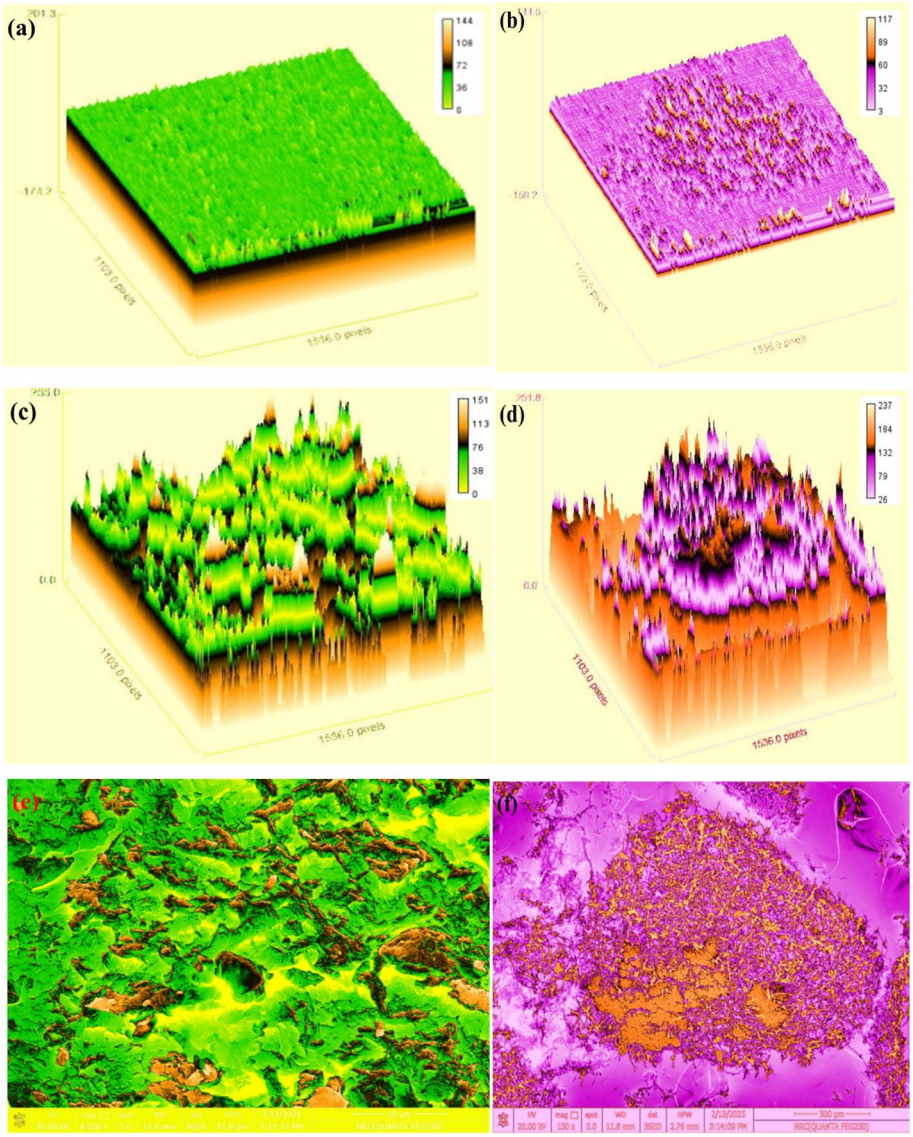

Fig. 5 SEM images analysis for surface roughness and waviness of raw RM after hormone loading RM/HP by the aid of programme Image J.

Table 1 Characterization of encapsulated formulation (HP-RM): particle size, zeta potential, and encapsulation efficiency of progesterone

				Encapsulation efficiency (EE%)
Formulation	Mean particle size	Dispersity (PDI)[a]	Zeta potential (mV)	Progesterone
Blank (RM)	50.20 ± 1.68 μm	Polymodal	−33.50 ± 1.21	—
HP-RM	512.00 ± 2.25 nm	Monomodal	−42.03 ± 1.63	98.10 ± 0.56

[a] Polymodal refers to PDI values that exceed 0.3, while monomodal refers to PDI values below 0.3.

mushroom matrix acting as a natural barrier, slowing down the diffusion of progesterone and ensuring prolonged delivery.[77] In contrast, the free progesterone showed a rapid and complete release in PBS, with 34.15 ± 1.46% released within 10 minutes and 100.09 ± 3.05% released within 2–4 hours, reflecting its unrestricted diffusion through the dialysis membrane. These findings highlight the effectiveness of the reishi mushroom matrix in controlling the release of progesterone, making it a promising candidate for applications requiring prolonged drug delivery, such as hormone replacement therapy or cancer treatment. Moreover, the pronounced sustained release in PBS compared to the limited release in SGF and SIF demonstrates the superiority of PBS as a release medium, as it maintains the structural integrity of the mushroom matrix and supports

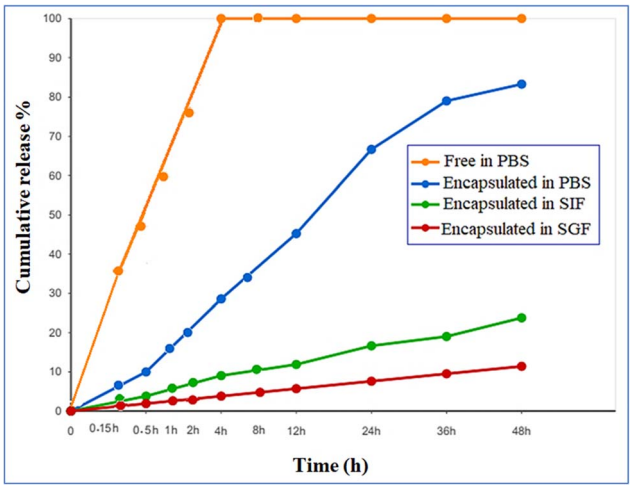

Fig. 6 *In vitro* release profiles of progesterone from reishi mushroom composite compared to free progesterone in different physiological media: PBS (pH 7.4), SIF (pH 6.8), and SGF (pH 1.2) over 48 hours. Values represent mean ± SD ($n = 3$).

optimal progesterone solubility and diffusion, closely mimicking systemic physiological conditions.[77–79]

3.3 *In vitro* kinetics

In this study, the *in vitro* release kinetics of encapsulated and free progesterone formulations were analyzed using various models to understand their release mechanisms, the invitro kinetics results were tabulated in Table 2. The *in vitro* release kinetic study comparing progesterone-loaded reishi mushroom and free progesterone highlights the superior controlled release properties of the reishi mushroom-based system. The zero-order model shows a higher release rate constant ($K_0 = 0.7567 \pm 1.15$) for encapsulated progesterone compared to free progesterone ($K_0 = 0.3469 \pm 1.10$), indicating a more sustained release. The first-order model reveals a much lower release rate constant ($K = 0.0002 \pm 0.52$) for encapsulated progesterone, suggesting prolonged release, while the Korsmeyer–Peppas model indicates a non-Fickian diffusion mechanism ($n = 0.4838 \pm 1.32$) for the encapsulated form, compared to the quasi-Fickian mechanism ($n = 0.1753 \pm 0.68$) of free progesterone. Additionally, the Higuchi model demonstrates a higher release rate constant ($K_h = 18.503 \pm 1.2$) for encapsulated progesterone, further confirming its efficient and sustained release. These findings underscore the reishi mushroom's ability to modulate progesterone release, making it an ideal drug carrier for sustained delivery in medical applications such as hormone replacement therapy and fertility treatments. Its natural polymeric matrix, biocompatibility, and biodegradability further enhance its potential as a safe and effective alternative to synthetic delivery systems (Fig. 7).

3.4 *In vitro* cytotoxicity and cell viability

3.4.1 Cytotoxicity and anti-cancer activity in MCF-7 cells (breast cancer cells). The MTT assay is utilized to evaluate the cytotoxic effects of progesterone loaded reishi mushroom composite on MCF-7 cells (breast cancer cells), in comparison to their free forms. After treating MCF-7 cells with different concentrations of progesterone loaded reishi mushroom composite, cell viability is quantified, and the potency of the treatment is determined by calculating the IC_{50} value. The IC_{50} value represents the concentration of a compound required to reduce cell viability by 50%, providing a measure of its effectiveness in inhibiting cell growth. In this study, the progesterone loaded reishi mushroom composite showed an IC_{50} value of 81.11 ± 1.95 μg mL^{-1}, which was lower than the IC_{50} values for the free forms of progesterone (123.12 ± 1.54 μg mL^{-1}) and reishi mushroom (70.21 ± 1.78 μg mL^{-1}). This indicates that the progesterone loaded reishi mushroom composite is more effective in reducing MCF-7 cell viability compared to the free progesterone. In this study, the progesterone–reishi mushroom composite exhibited an IC_{50} of 81.11 μg mL^{-1} against MCF-7 breast cancer cells, which is a significant improvement over free progesterone ($IC_{50} = 123.12$ μg mL^{-1}). Although the progesterone–reishi mushroom composite exhibited a significantly lower IC_{50} value (81.11 μg mL^{-1}) against MCF-7 breast cancer cells compared to free progesterone (123.12 μg mL^{-1}), it is important to contextualize these findings by comparing them with the IC_{50} values of standard clinical anti-cancer drugs. Common chemotherapeutics such as doxorubicin and paclitaxel typically display much lower IC_{50} values in MCF-7 cells, often in the range of 0.01–2 μg mL^{-1}. For example, doxorubicin has been reported to have an IC_{50} of approximately 0.5–1.0 μg mL^{-1}, and paclitaxel an IC_{50} of about 0.006–0.2 μg mL^{-1} in MCF-7 cells.[80–83] While the composite's cytotoxic potency is lower than these conventional agents, its natural composition and potential for reduced toxicity may offer advantages for combination therapies or for patients seeking alternatives to standard chemotherapy. A lower IC_{50} value for the progesterone loaded reishi mushroom composite suggests that a smaller concentration of the

Table 2 Comparison of release kinetic parameters for progesterone loaded reishi mushroom and free progesterone

		Active ingredients	
Release kinetic model	Parameters	Encapsulated progesterone	Free progesterone
Zero-order model	K_0	0.7567 ± 1.15	0.3469 ± 1.10
First-order model	K	0.0002 ± 0.52	0.0115 ± 0.75
Korsmeyer–Peppas model	K	0.2267 ± 2.02	0.652 ± 1.23
	n	0.4838 ± 1.32	0.1753 ± 0.68
Higuchi model	K_H	18.503 ± 1.2	11.94 ± 1.5

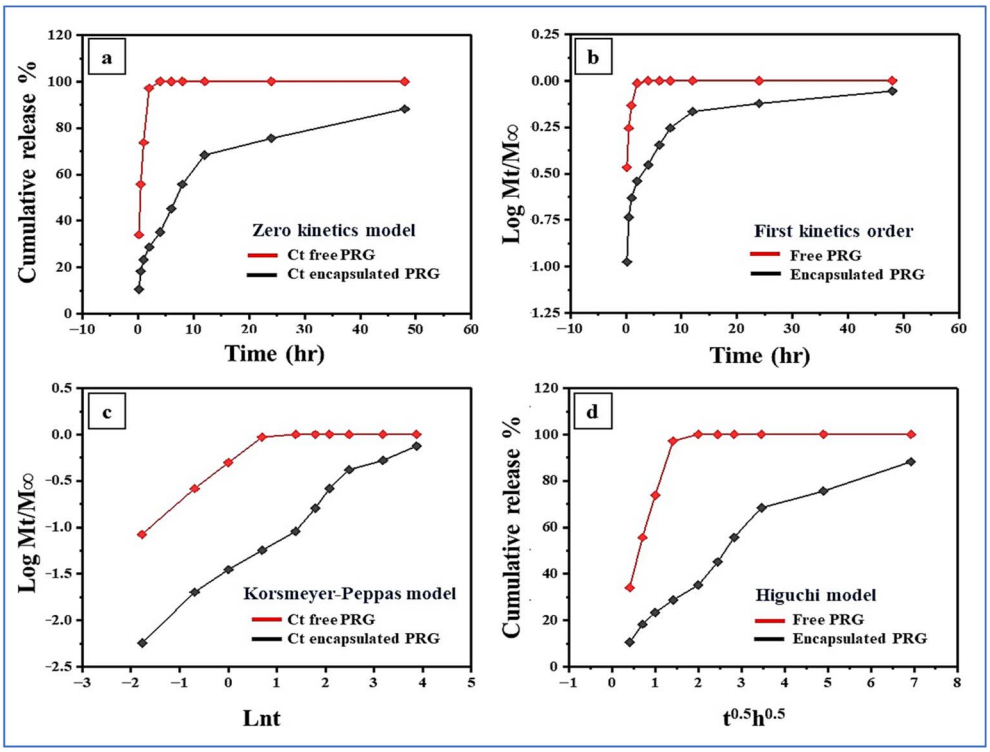

Fig. 7 The release kinetics of progesterone from both encapsulated and free forms using four different kinetic models: (a) zero-order, (b) first-order, (c) Korsmeyer–Peppas, and (d) Higuchi.

combination is required to achieve 50% inhibition of cell viability, highlighting its increased potency. The loading of progesterone in reishi mushroom likely enhances their delivery and bioavailability, allowing for greater therapeutic efficacy at lower doses. On the other hand, the free form of progesterone requires higher concentrations to achieve the same level of inhibition, which may lead to limitations in their clinical effectiveness and a higher likelihood of side effects. The results demonstrate that Reishi mushroom-based delivery enhances the stability and targeting of progesterone, offering a more effective breast cancer treatment with lower dosages, as shown in Fig. 8. This supports further development of reishi mushroom-based formulations in Hormone replacement and cancer therapy. Statistical analysis was conducted using one-way ANOVA followed by Tukey's post hoc test to compare the IC_{50} values of free progesterone (HP), reishi mushroom (RM), and the progesterone–reishi mushroom composite (HP-RM) against MCF-7 cells. Both RM (70.21 ± 1.78 μg mL^{-1}) and HP-RM (81.11 ± 1.95 μg mL^{-1}) exhibited significantly lower IC_{50} values compared to HP (123.12 ± 1.54 μg mL^{-1}) ($p < 0.001$ for both), indicating enhanced cytotoxicity against breast cancer cells. However, there was no statistically significant difference between RM and HP-RM ($p = 0.09$), suggesting that the incorporation of progesterone did not significantly augment the cytotoxic effect beyond that provided by the reishi mushroom alone. These findings imply that the cytotoxic activity of the composite formulation is predominantly attributed to the bioactive components of the reishi mushroom matrix. The data are summarized in Table 3.

Values are presented as mean ± SD ($n = 3$). Statistical significance was determined by one-way ANOVA with Tukey's *post hoc* test.

3.5 Molecular docking study

3.5.1 Binding affinities of ganoderic acid A and progesterone. The binding affinities (ΔG, kcal mol^{-1}) of ganoderic acid A and progesterone for each target receptor are summarized in

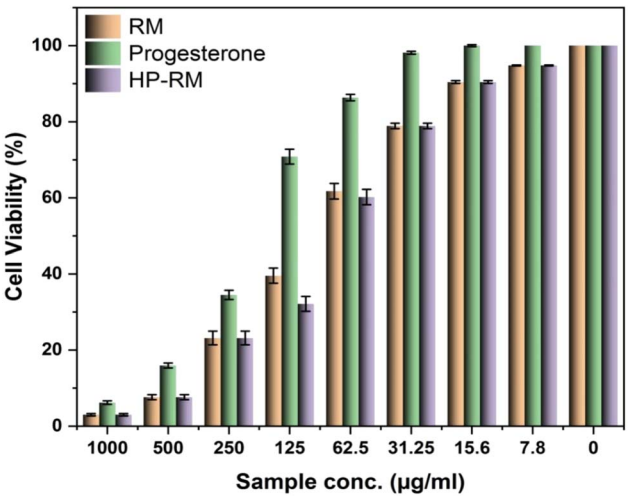

Fig. 8 Cytotoxicity and anti-cancer activity of reishi mushroom, progesterone and progesterone-loaded reishi mushroom composite in MCF-7 breast cancer cells.

Table 3 IC_{50} values of tested formulations against MCF-7 cells and statistical significance[a]

Group	IC_{50} (μg mL^{-1})	Significance *vs.* HP	Significance *vs.* RM
Free progesterone (HP)	123.12 ± 1.54	N/A	N/A
Reishi mushroom (RM)	70.21 ± 1.78	$p < 0.001$	N/A
Progesterone–reishi mushroom composite	81.11 ± 1.95	$p < 0.001$	$p = 0.09$

[a] N/A: not applicable.

Table 4 Binding affinities of ganoderic acid A and progesterone

Receptor	Ligand	Binding affinity (kcal mol^{-1})
PCL-2	Ganoderic acid A	−8
	Progesterone	−7.8
PI3K	Ganoderic acid A	−9.5
	Progesterone	−8.3
PR	Ganoderic acid A	−8.6
	Progesterone	−8.2
ERα	Ganoderic acid A	−8.6
	Progesterone	−7.3

Table 4. Ganoderic acid A exhibited stronger binding affinities compared to progesterone across all receptors, with the highest affinity observed for PI3K (−9.5 kcal mol^{-1}).

3.5.2 Molecular interactions

3.5.2.1 PCL-2 interactions. Ganoderic acid A formed multiple conventional hydrogen bonds with ARG A:137, ASN A:86, and GLN A:45, indicating stable binding through polar interactions. These hydrogen bonds likely contribute to the ligand's affinity for PCL-2, reinforcing its potential bioactivity. An unfavorable acceptor–acceptor interaction with ARG A:42 was also observed indicating steric or electronic repulsion at that site (Fig. 9). Whereas, progesterone exhibited a single alkyl interaction with ILE A:114, suggesting hydrophobic stabilization within the binding pocket (Fig. 10). Overall, the presence of strong hydrogen bonding interactions suggests that ganoderic acid A could effectively engage with PCL-2, potentially influencing its biological activity in hormone regulation or therapeutic pathways.

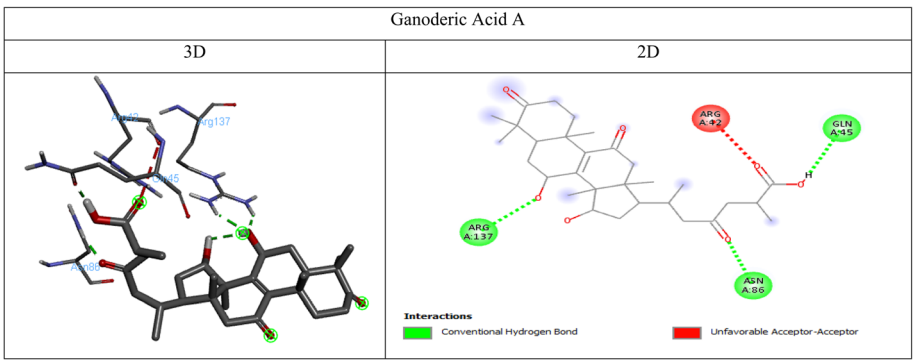

Fig. 9 3D and 2D visualizations of the interactions between PCL-2 and ganoderic acid A.

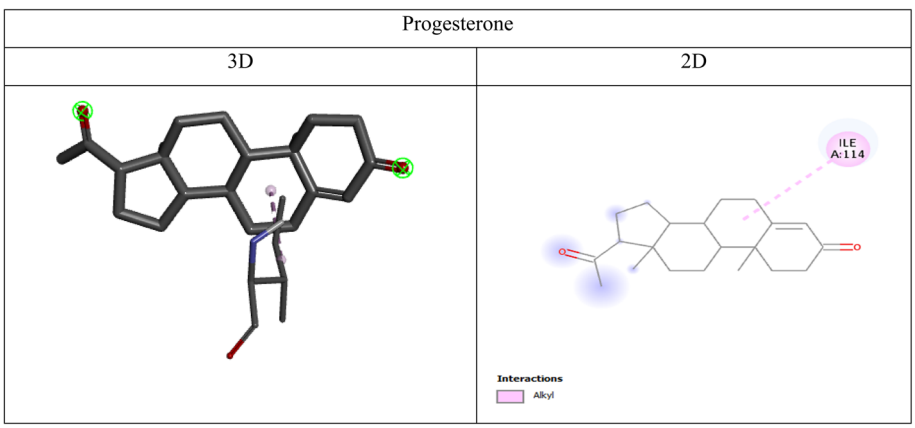

Fig. 10 3D and 2D visualizations of the interactions between PCL-2 and progesterone.

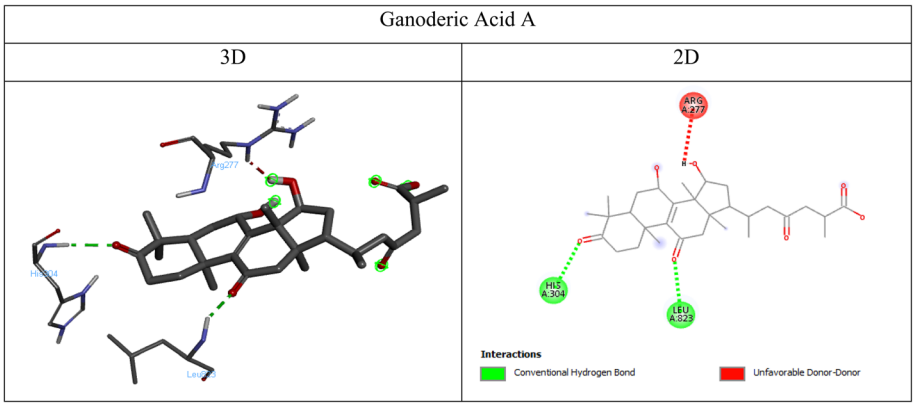

Fig. 11 3D and 2D visualizations of the interactions between PI3K and ganoderic acid A.

3.5.2.2 PI3K interactions. Ganoderic acid A established conventional hydrogen bonds with HIS A:304 and LEU A:323, suggesting strong polar interactions that contribute to its binding stability within the active site of PI3K along with an unfavorable donor–donor interaction with ARG A:277 indicating potential steric or electronic repulsion that might slightly reduce binding efficiency (Fig. 11). The presence of multiple hydrogen bonds suggests that ganoderic acid A could effectively interact with PI3K. Whereas, progesterone formed a single conventional hydrogen bond between the C=O group of progesterone and the HIS A:304 residue in the PI3K binding site, indicating weaker binding compared to ganoderic acid A (Fig. 12).

3.5.2.3 Progesterone receptor (PR) interactions. Ganoderic acid A displayed multiple conventional hydrogen bonds with SER B:910, SER A:910, ILE A:896, PHE A:895, and PHE A:905 suggesting strong binding stability, alongside an unfavorable donor–donor interaction with SER A:898 (Fig. 13), these interactions indicate that ganoderic acid A could potentially influence progesterone receptor activity by exhibiting competitive binding, which might impact hormonal regulation and signaling pathways. Whereas, progesterone formed a conventional hydrogen bond with GLN A:747 and alkyl interactions with VAL A:730, ILE A:748, and ILE A:751, indicating hydrophobic stabilization (Fig. 14).

3.5.2.4 Estrogen receptor alpha (ERα) interactions. Ganoderic acid A demonstrated a conventional hydrogen bond with SER B:468 indicating a stabilizing interaction essential for ligand binding. However, the presence of an unfavorable donor–donor interaction with LEU B:462 suggests potential steric or electronic hindrance that may slightly affect binding efficiency (Fig. 15). Whereas, progesterone exhibited a conventional hydrogen bond with LYS B:467 suggesting a stabilizing interaction crucial for ligand binding. Additionally, a pi–sigma interaction with HIS B:377 is observed, indicating possible π-electron cloud interactions that might contribute to ligand stabilization within the binding pocket (Fig. 16).

3.6 Antimicrobial assays

3.6.1 Antimicrobial activity of reishi mushroom and HP-RM. According to Table 6 and Fig. 17, the results indicated no statistically significant difference in the antimicrobial activity of reishi mushroom and HP-RM against various microbial pathogens ($P < 0.05$). HP-RM demonstrated a wider zone of inhibition against Gram-positive pathogens, with *Streptococcus*

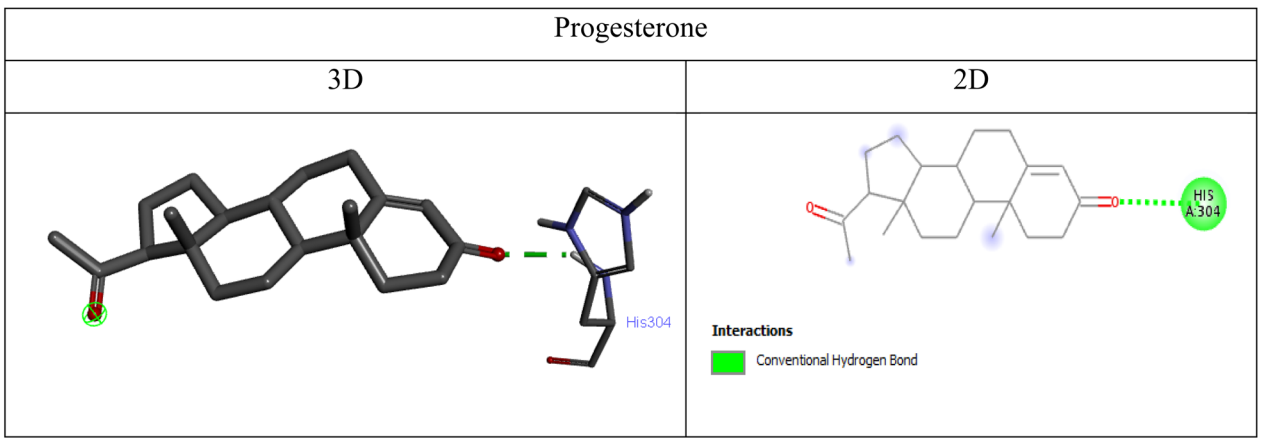

Fig. 12 3D and 2D visualizations of the interactions between PI3K and progesterone.

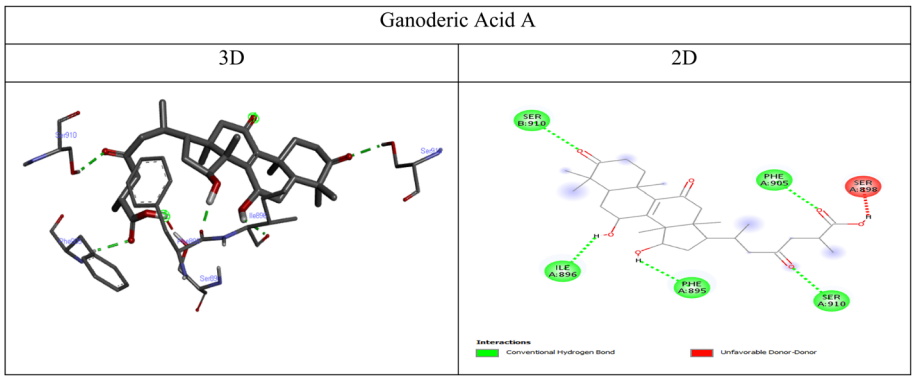

Fig. 13 3D and 2D visualizations of the interactions between progesterone receptor and ganoderic acid A.

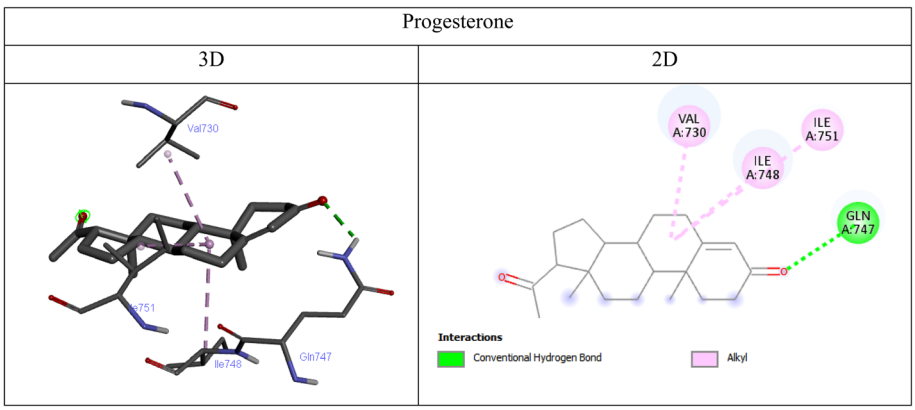

Fig. 14 3D and 2D visualizations of the interactions between progesterone receptor and progesterone.

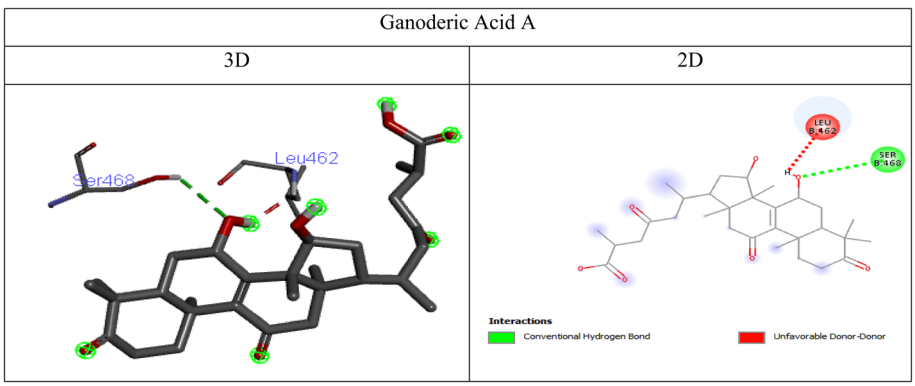

Fig. 15 3D and 2D visualizations of the interactions between estrogen receptor alpha (ERα) and ganoderic acid A.

agalactiae (19.33 ± 2.40 mm) and *Staphylococcus aureus* (17.00 ± 2.08 mm) showing greater sensitivity compared to Gram-negative bacteria and *Candida albicans*. Similar inhibitory zones were observed for *Klebsiella pneumoniae* (12.67 ± 1.76 mm) and *C. albicans* (12.67 ± 0.67 mm). HP-RM also exhibited lower MIC and MBC values for Gram-positive bacteria, with *Str. agalactiae* (41.60 ± 10.30 μg mL^{-1} and 52.10 ± 10.40 μg mL^{-1}, respectively) and *S. aureus* (52.10 ± 10.40 μg mL^{-1} and 72.93 ± 27.55 μg mL^{-1}, respectively) being more susceptible than Gram-negative bacteria and *C. albicans*. *K. pneumoniae* showed comparable MBC (104.17 ± 20.83 μg mL^{-1}) and MIC values, as shown in Table 5. The MBC/MIC ratio for both HP-RM and reishi mushroom was less than 4, suggesting bactericidal effects against the tested pathogens.

3.6.2 Comparison with previous studies

3.6.2.1 Progesterone and its derivatives. Kalaycı-Yüksek *et al.* (2021) highlighted the antimicrobial potential of progesterone,[84] while Doğan *et al.* (2017) reported its inability to

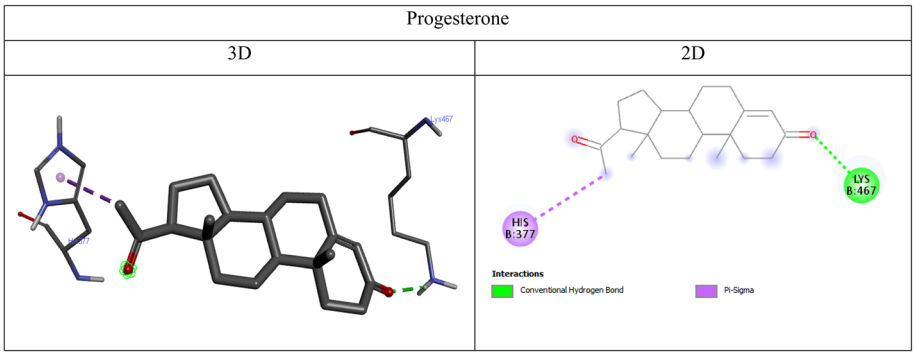

Fig. 16 3D and 2D visualizations of the interactions between estrogen receptor alpha (ERα) and progesterone.

Table 5 Zone of inhibition of progesterone hormone and encapsulating formula (HP-RM) against different microbial species[a]

	Zone of inhibition	
Tested organisms	Reishi mushroom	Encapsulating formula
Str. agalactiae	15.00 ± 1.73	19.33 ± 2.40
S. aureus	13.33 ± 1.76	17.00 ± 2.08
E. coli	12.00 ± 2.31	16.00 ± 2.31
K. puemoniae	9.33 ± 1.76	12.67 ± 1.76
C. albicans	10.00 ± 1.15	12.67 ± 0.67

[a] Data are expressed as means ± SE * significant difference at $P < 0.05$.

inhibit *S. aureus* and *E. coli*.[85] The presence of amino linkage (–N=C–) in progesterone derivatives has been linked to enhanced antimicrobial activity against Gram-positive (*S. aureus*), Gram-negative (*E. coli*), and fungal pathogens.[86–88] Gurgan *et al.* (1993) attributed the antibacterial effects of progesterone to lysozyme enzymes, which disrupt microbial cell walls.[89]

3.6.2.2 Reishi mushroom extracts. Reishi mushroom acetone and methanol extracts demonstrated significant antibacterial activity against *K. pneumoniae* (31.60 ± 0.10 mm and 21.30 ± 0.06 mm, respectively), *E. coli* (27.40 ± 0.19 mm and 20.10 ± 0.20 mm, respectively), and *S. aureus* (18.00 ± 0.20 mm and 16.30 ± 0.20 mm, respectively). The MIC values for *K. pneumoniae*, *E. coli*, and *S. aureus* were 4.33 ± 0.33 mg mL^{-1}, 8.17 ± 0.48 mg mL^{-1}, and 19.00 ± 0.00 mg mL^{-1}, respectively. Kamra and Bhatt (2012) reported similar findings, with reishi mushroom extracts showing a MIC of 31.3 μg mL^{-1} against *K. pneumoniae*.[57] Daruliza *et al.* (2012) noted the antifungal activity of methanolic reishi mushroom extract against *C. albicans* (MIC: 3.125 mg mL^{-1}, inhibition zone: 12.8 ± 0.25 mm),[90] while Roy *et al.* (2016) found no antifungal activity in ethyl acetate extracts.[91]

3.6.3 Mechanisms of antimicrobial action. Reishi mushroom contains bioactive compounds such as lectins, polysaccharides, triterpenoids, ganoderic acid, terpenes, and ganomycin, which contribute to its antimicrobial properties.[92] These compounds inhibit critical cellular processes, including oxygen uptake, oxidative phosphorylation, and DNA production,[93,94] thereby preventing microbial growth and multiplication. Terpenes, in particular, are thermally stable and have a prolonged half-life in the host body. Ganoderic acid exhibits stronger antibacterial activity against Gram-positive bacteria than Gram-negative bacteria.[95] Ergosta-5,7,22-triene-3β,14α-diol, extracted from reishi mushroom, has shown remarkable effectiveness against methicillin-resistant *S. aureus* (MRSA) and *Streptococcus pyogenes*.[96] Additionally, reishi mushroom extracts have demonstrated superior antibacterial effects compared to antibiotics like penicillin and streptomycin, highlighting their potential for disease prevention and treatment.[97] The anticandidal activity of reishi mushroom is attributed to its ability to suppress mycelium development.[98]

3.6.4 Antimicrobial and oncological relevance. The antimicrobial activity of the progesterone–reishi mushroom (HP-RM) composite represents a significant advancement in the development of multifunctional therapeutic agents. The results

Table 6 MIC, MBC and MIC/MBC ratios of progesterone hormone and encapsulating formula against different microbial species[a]

	Reishi mushroom (μg mL^{-1})			HP-RM (μg mL^{-1})		
Tested organisms	MIC	MBC	MBC/MIC ratio	MIC	MBC	MBC/MIC ratio
Str. Agalactiae	83.33 ± 20.83	145.83 ± 55.12	1.7	41.60 ± 10.30	52.10 ± 10.40	1.3
S. aureus	83.33 ± 20.83	145.83 ± 55.12	1.7	52.10 ± 10.40	72.93 ± 27.55	1.4
E. coli	166.67 ± 41.67	250.00 ± 125.00	1.5	83.33 ± 20.83	104.17 ± 20.83	1.2
K. puemoniae	104.17 ± 20.83	166.67 ± 41.67	1.6	104.17 ± 20.83	104.17 ± 20.83	1
C. albicans	104.17 ± 20.83	145.83 ± 55.12	1.4	83.10 ± 10.40	105.17 ± 19.83	1.3

[a] Data are expressed as means ± SE * significant difference at $P < 0.05$.

highlight the composite's potent activity against Gram-positive pathogens, such as *Streptococcus agalactiae* and *Staphylococcus aureus*, with zones of inhibition measuring 19.33 ± 2.40 mm and 17.00 ± 2.08 mm, respectively. This enhanced activity compared to plain reishi mushroom suggests a synergistic interaction between progesterone and the bioactive components of the mushroom, which may disrupt microbial cell walls and inhibit critical cellular processes such as oxygen uptake and DNA production. The lower MIC and MBC values for HP-RM against Gram-positive bacteria (*e.g.*, *Str. Agalactiae*: MIC = 41.60 ± 10.30 μg mL; MBC = 52.10 ± 10.40 μg mL^{-1}) further underscore its efficacy, as these values indicate the composite's ability to inhibit and kill pathogens at lower concentrations. The MBC/MIC ratios for HP-RM, consistently below 4, confirm its bactericidal nature, a critical attribute for therapeutic applications. The composite also demonstrated notable activity against Gram-negative bacteria and *Candida albicans*, albeit with slightly reduced efficacy compared to Gram-positive pathogens. For instance, inhibitory zones of 16.00 ± 2.31 mm for *E. coli* and 12.67 ± 0.67 mm for *C. albicans* were observed, with MIC values of 83.33 ± 20.83 μg mL^{-1} and 83.10 ± 10.40 μg mL^{-1}, respectively. This aligns with previous studies that have reported the antimicrobial potential of reishi mushroom extracts against Gram-negative bacteria and fungi, albeit with varying degrees of effectiveness. The observed differences in activity between Gram-positive and Gram-negative bacteria may be attributed to the structural complexity of Gram-negative cell walls, which contain an outer membrane that limits the penetration of antimicrobial agents. However, the presence of ganoderic acid and other triterpenoids in the composite likely enhances its ability to disrupt microbial membranes, even in Gram-negative species. The antimicrobial mechanisms of HP-RM can be further elucidated by considering the individual contributions of its components. Progesterone, though not traditionally recognized for its antimicrobial properties, has been shown to exhibit activity against certain pathogens, particularly when modified or combined with other bioactive compounds. The encapsulation of progesterone within the reishi mushroom matrix may enhance its stability and bioavailability, thereby amplifying its antimicrobial effects. Additionally, the bioactive compounds in reishi mushroom, such as terpenes and ganoderic acid, are known to exhibit strong antibacterial and antifungal properties, particularly against Gram-positive bacteria and fungi. These compounds likely act synergistically with progesterone to enhance the overall antimicrobial efficacy of the composite. In comparison to previous studies, the antimicrobial activity of HP-RM is consistent with findings that highlight the potential of reishi mushroom extracts as natural antimicrobial agents. For example, reishi mushroom extracts have been reported to exhibit significant antibacterial activity against *Klebsiella pneumoniae* and antifungal activity against *C. albicans*. The results of this study build on these findings by demonstrating that the encapsulation of progesterone within the reishi mushroom matrix not only retains but enhances the antimicrobial properties of the individual components. This suggests that HP-RM could serve as a promising alternative to conventional antimicrobial agents, particularly in the context of multidrug-resistant pathogens. In conclusion, the antimicrobial assays conducted in this study highlight the potential of the progesterone–reishi mushroom composite as a multifunctional therapeutic agent with broad-spectrum antimicrobial activity. The composite's ability to inhibit and kill Gram-positive pathogens, coupled with its moderate activity against Gram-negative bacteria and fungi, underscores its potential for applications in both medical and pharmaceutical contexts. Future studies could explore the mechanisms underlying the synergistic effects of progesterone and reishi mushroom bioactive compounds, as well as the potential for HP-RM to be incorporated into topical or systemic antimicrobial formulations. The simultaneous administration of antibacterial and anti-cancer treatments is often necessary in several scenarios encountered in oncology practice. Cancer patients, especially those undergoing chemotherapy, radiotherapy, or immunosuppressive therapies, are at increased risk of developing bacterial infections due to compromised immune function. For example, in cases of febrile neutropenia-a common and potentially life-threatening complication in patients receiving cytotoxic chemotherapy-prompt empirical antibacterial therapy is essential and is administered concurrently with ongoing anti-cancer treatment to prevent severe infectious complications. Additionally, certain cancers may become secondarily infected, particularly when tumors ulcerate, become necrotic, or are associated with chronic wounds, as seen in advanced breast or head and neck cancers. In such cases, antibacterial therapy is required alongside anti-cancer treatment to manage local or systemic infections. Post-surgical infections, device-related infections (*e.g.*, central venous catheters), and infections following invasive procedures are also common in cancer patients and necessitate combined therapeutic approaches. Furthermore, in specific malignancies with an infectious etiology, such as gastric MALT lymphoma associated with Helicobacter pylori, eradication of the causative bacteria using antibiotics is an integral part of the anti-cancer regimen. Prophylactic antibiotics may also be administered to high-risk patients, such as those undergoing hematopoietic stem cell transplantation, to prevent opportunistic infections during periods of profound immunosuppression. The development of therapeutic agents, such as the progesterone–reishi mushroom composite described in our study, that possess both anticancer and antimicrobial properties, may offer additional benefits for immunocompromised cancer patients by simultaneously addressing tumor progression and infection risk. We have clarified these points in the revised manuscript to highlight the clinical relevance of dual-action therapies in oncology.

3.7 Results of accelerated stability study

3.7.1 Stability of progesterone–reishi mushroom composite. At time zero, the composite exhibited high progesterone loading efficiency (98.10%), uniform particle size, and a zeta potential indicating good colloidal stability, consistent with previous biopolymer-based encapsulation studies.[51] After 3 months, the progesterone content remained at 96.8%, particle

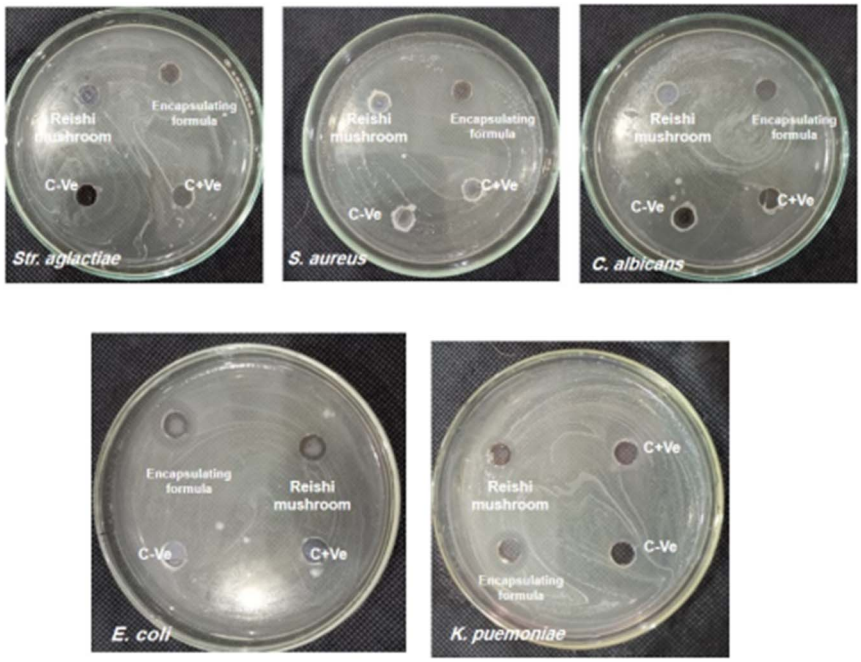

Fig. 17 Zone of inhibition of reishi mushroom and encapsulating formula against different microbial species.

size showed a slight increase, and zeta potential decreased marginally, yet no aggregation or sedimentation was observed the cumulative release over 48 hours decreased slightly to 86.4% (*vs.* 88.25% at zero time), indicating sustained release capability was largely retained.[54,99,100] At 6 months, the composite retained 94.2% of its initial progesterone content. Physical and parameters remained stable. The cumulative release declined slightly to 83.7%, as illustrated in Table 7 and Fig. 18a–d and 19a–d. These findings align with other reports on the stability of natural polymer-based systems under accelerated conditions.[57,101,102]

3.7.2 Antimicrobial activity of the progesterone–reishi mushroom composite during accelerated stability testing. The antimicrobial activity of the progesterone–reishi mushroom composite (HP-RM) was systematically assessed at zero time, 3 months, and 6 months during accelerated stability testing (40 °C ± 2 °C/75% ± 5% RH). The results, presented in Table 8, demonstrate the composite's broad-spectrum antimicrobial efficacy and its robust retention over the entire storage period. At the initial time point, HP-RM exhibited potent inhibitory and bactericidal/fungicidal activity against both Gram-positive and Gram-negative bacteria, as well as *Candida albicans*. The minimum inhibitory concentration (MIC) for streptococcus agalactiae was 41.60 ± 10.30 μg mL^{-1}, with a corresponding minimum bactericidal concentration (MBC) of 52.10 ± 10.40 μg mL^{-1} and an MBC/MIC ratio of 1.3. For *Staphylococcus aureus*, the MIC was 52.10 ± 10.40 μg mL^{-1}, MBC was 72.93 ± 27.55 μg mL^{-1}, and the MBC/MIC ratio was 1.4. Against *Escherichia coli* and *Klebsiella pneumoniae*, the MIC values were 83.33 ± 20.83 μg mL^{-1} and 104.17 ± 20.83 μg mL^{-1}, respectively, with corresponding MBC/MIC ratios of 1.2 and 1.0. The composite also demonstrated antifungal activity against *C. albicans* (MIC = 83.10 ± 10.40 μg mL^{-1}, MFC = 105.17 ± 19.83 μg mL^{-1}, MFC/MIC = 1.3). After 3 months of accelerated storage, all tested organisms showed only minor increases in MIC and MBC/MFC values. The MIC for *S. agalactiae* increased to 43.40 ± 10.80 μg mL^{-1}, and for *S. aureus* to 53.90 ± 10.85 μg mL^{-1}, with MBC/MIC ratios remaining unchanged. Similar trends were observed for *E. coli*, *K. pneumoniae*, and C. albicans, indicating that the composite retained its antimicrobial potency at this

Table 7 Stability and characterization parameters of progesterone–reishi mushroom composite (HP-RM) under accelerated conditions (40 °C ± 2 °C/75% ± 5% RH)[a]

Parameter	Zero time	3 months	6 months
Progesterone content (%)	98.10 ± 1.2	96.80 ± 1.5	94.20 ± 1.8
Mean particle size (μm)	512.00 ± 2.25 nm	515 ± 0.40	520.05 ± 0.50
Polydispersity index (PDI)	Monomodal	Monomodal	Polymodal
Zeta potential (mV)	−42.03 ± 1.63	−39.7 ± 1.3	−35.1 ± 1.5
Encapsulation efficiency (%)	98.10 ± 0.56	97.10 ± 0.67	95.80 ± 0.74
48 h cumulative release (%)	88.25 ± 2.1	86.40 ± 2.3	83.70 ± 2.6

[a] All values are expressed as mean ± SD ($n = 3$).

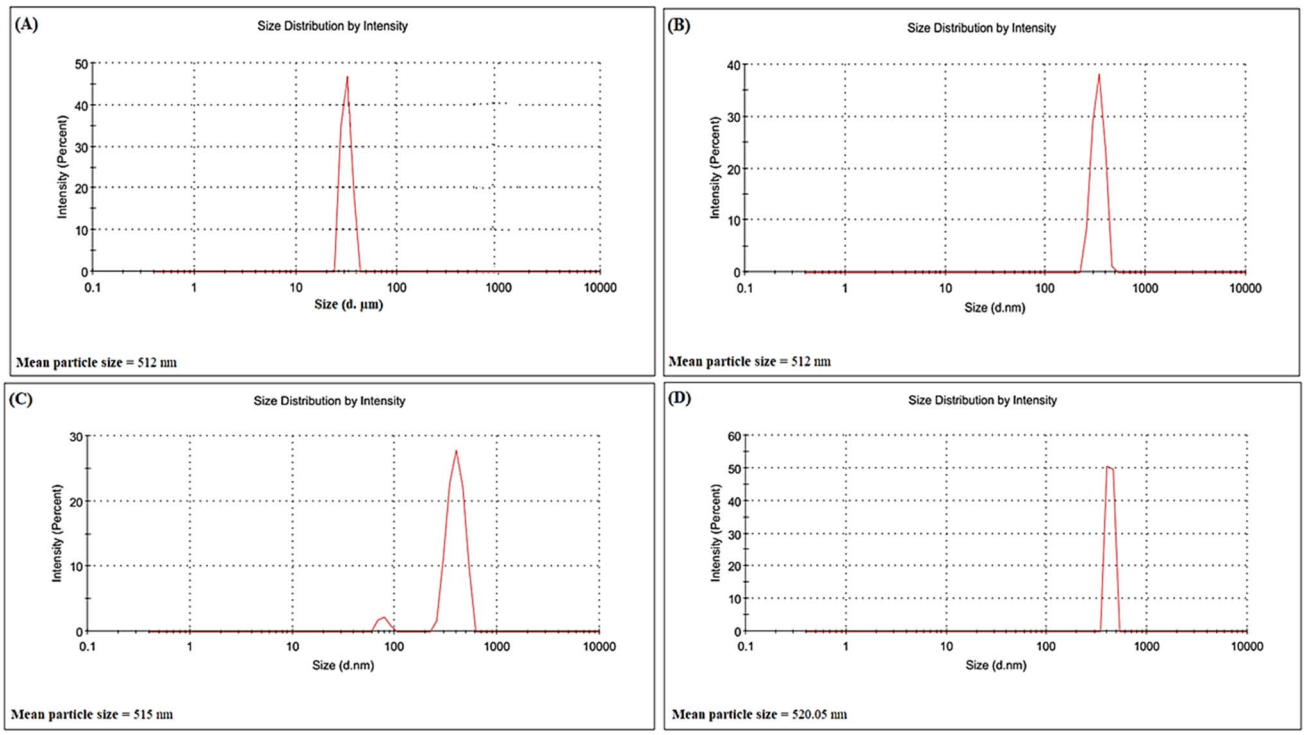

Fig. 18 Particle size distribution curves of (A) the blank reishi mushroom *vs.* HP-RM at different time intervals (B) zerotime (0 months), (C) accelerated 3 months and (D) accelerated 6 months.

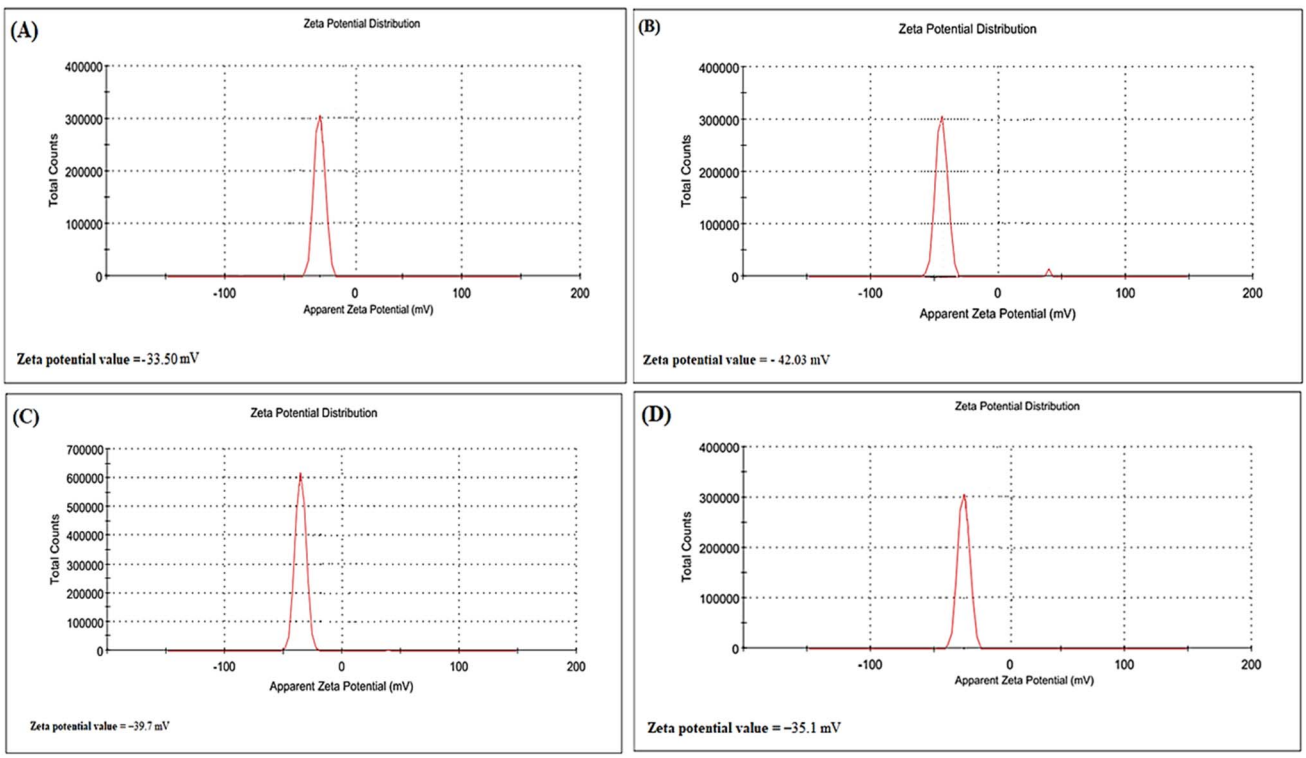

Fig. 19 Zeta potential curves of (A) the blank reishi mushroom *vs.* HP-RM at different time intervals (B) zerotime, (C) accelerated 3 months and (D) accelerated 6 months.

Table 8 Antimicrobial activity of progesterone–reishi mushroom composite (HP-RM) during accelerated stability testing (40 °C ± 2 °C/75% ± 5% RH)[a]

Tested organism	Parameter	Zero time	3 months	6 months
Str. Agalactiae	MIC (μg mL^{-1})	41.60 ± 10.30	43.40 ± 10.80	45.10 ± 11.20
	MBC (μg mL^{-1})	52.10 ± 10.40	55.20 ± 11.10	58.70 ± 12.15
	MBC/MIC ratio	1.3	1.3	1.3
S. aureus	MIC (μg mL^{-1})	52.10 ± 10.40	53.90 ± 10.85	55.80 ± 11.30
	MBC (μg mL^{-1})	72.93 ± 27.55	75.60 ± 28.30	78.20 ± 29.45
	MBC/MIC ratio	1.4	1.4	1.4
E. coli	MIC (μg mL^{-1})	83.33 ± 20.83	86.50 ± 21.60	89.75 ± 22.40
	MBC (μg mL^{-1})	104.17 ± 20.83	108.10 ± 21.65	112.30 ± 22.90
	MBC/MIC ratio	1.2	1.2	1.3
K. pneumoniae	MIC (μg mL^{-1})	104.17 ± 20.83	108.10 ± 21.65	112.30 ± 22.90
	MBC (μg mL^{-1})	104.17 ± 20.83	108.10 ± 21.65	112.30 ± 22.90
	MBC/MIC ratio	1.0	1.0	1.0
C. Albicans	MIC (μg mL^{-1})	83.10 ± 10.40	86.30 ± 11.10	89.50 ± 11.70
	MFC (μg mL^{-1})	105.17 ± 19.83	109.20 ± 20.60	113.40 ± 21.90
	MFC/MIC ratio	1.3	1.3	1.3

[a] All values are expressed as mean ± SD ($n = 3$).

intermediate time point. At 6 months, the HP-RM composite continued to exhibit strong antimicrobial activity, with MIC and MBC/MFC values showing only modest further increases compared to the initial and 3 month values, where the MIC for *S. agalactiae* was 45.10 ± 11.20 μg mL^{-1}, and for *S. aureus* was 55.80 ± 11.30 μg mL^{-1}. All MBC/MIC and MFC/MIC ratios remained well below 4 throughout the study, confirming the continued bactericidal and fungicidal efficacy of the composite.[103] Overall, these results demonstrate that the progesterone–reishi mushroom composite maintains its broad-spectrum antimicrobial activity throughout six months of accelerated storage, with only minimal reductions in potency.[57,101,104] This stability is indicative of the composite's potential for long-term pharmaceutical applications requiring both hormonal and antimicrobial effects.

3.8 Study limitation and future perspective

A key limitation of the present study is that all *Ganoderma lucidum* (Reishi mushroom) fruiting bodies were sourced from a single commercial batch to ensure material consistency and minimize variability during the experimental procedures. While this approach enhances reproducibility within the current study, it does not account for potential batch-to-batch differences that may arise due to variations in cultivation conditions, harvest time, or processing methods. Such variability could influence the physicochemical properties and bioactive compound content of the mushroom matrix, potentially affecting encapsulation efficiency, drug release profiles, and biological activity. Therefore, future studies should include the evaluation of multiple independent batches of *Ganoderma lucidum*, accompanied by comprehensive compositional profiling-such as quantification of key bioactive constituents (*e.g.*, polysaccharides, triterpenoids)-to assess the robustness and generalizability of the encapsulation approach. Another important limitation is that the current research was restricted to *in vitro* experiments (cytotoxicity and antibacterial assays). While these findings provide valuable initial insights, they do not fully represent the complex interactions, pharmacodynamics, and potential toxicological effects that may occur *in vivo*. Therefore, future research should include animal experiments to investigate the *in vivo* pharmacokinetics, biodistribution, therapeutic efficacy, and safety profile of the progesterone–reishi mushroom composite in relevant models. Such studies are essential to validate the translational potential of this delivery system and to address key questions regarding its biocompatibility, metabolism, and long-term effects. Additionally, the cytotoxicity evaluation in this study was limited to a single tumor cell line (MCF-7 breast cancer cells). To better understand the spectrum and selectivity of the composite's anticancer activity, future studies should assess its cytotoxic effects against a broader panel of tumor cell lines, including both hormone-dependent (*e.g.*, T47D, LNCaP) and hormone-independent (*e.g.*, MDA-MB-231, HeLa, A549) cancers. This would provide a more comprehensive assessment of its therapeutic potential and possible mechanisms of action. Further research should also explore the scalability of the encapsulation process. These findings highlight the need for further optimization and *in vivo* studies to fully assess the therapeutic potential and clinical applicability of the progesterone–reishi mushroom composite. Addressing these aspects will be essential for translating this innovative delivery system into practical applications for hormone replacement therapy and targeted anticancer treatment.

4 Conclusion

This study addresses the limitations of conventional hormone replacement therapy (HRT) and hormone-dependent cancer treatments by developing an innovative progesterone–reishi mushroom (*Ganoderma lucidum*) composite. Encapsulating progesterone within the reishi mushroom matrix enhances its bioavailability, stability, and targeted delivery while minimizing

side effects. The composite demonstrates sustained release, ensuring prolonged therapeutic action, and exhibits superior anticancer activity compared to free progesterone, making it a promising candidate for lower-dose, high-efficacy treatments. Molecular docking studies reveal the synergistic potential of progesterone and ganoderic acid A, a bioactive compound in reishi mushroom, in modulating hormone receptors and inhibiting cancer progression. Additionally, the composite shows significant antimicrobial activity, particularly against Gram-positive pathogens, highlighting its multifunctional therapeutic potential. By integrating natural bioactive compounds with synthetic hormones, this research offers a safer, more effective, and targeted approach to therapy. The progesterone–reishi mushroom composite represents a significant advancement in drug delivery, combining hormonal regulation with anticancer and antimicrobial properties, and paving the way for novel treatments in women's health and cancer therapy. Furthermore, its physicochemical and functional robustness under accelerated storage conditions (40 °C ± 2 °C/75% ± 5% RH) confirms the stability of the formulation, reinforcing its potential for pharmaceutical applications.

Consent for publication

The authors confirm: this work represents original research that has not been previously published in any form; this manuscript has not been submitted for review or publication consideration elsewhere; the publication has received approval from all co-authors.

Ethics approval and consent to participate

Not applicable, as the study did not apply to human or animal studies. The article does not include any studies on human participants or animals conducted by any of the authors.

Data availability

The authors declare that the data supporting the findings of this study are available within the article.

Conflicts of interest

All authors declare that they have no conflicts of interest to disclose.

Acknowledgements

This work was supported and funded by the Deanship of Scientific Research at Imam Mohammad Ibn Saud Islamic University (IMSIU) (grant number IMSIU-DDRSP2501).

References

1 K. Vigneswaran and H. Hamoda, Hormone replacement therapy–Current recommendations, *Best Pract. Res. Clin. Obstet. Gynaecol.*, 2022, **81**, 8–21.
2 C. Bulletti, F. M. Bulletti, R. Sciorio and M. Guido, Progesterone: the key factor of the beginning of life, *Int. J. Mol. Sci.*, 2022, **23**, 14138.
3 M. O. F. Khan and C. Llayton, Hormoneal Therapy, in *Med. Chem. Pharm. Students*, Bentham Science Publishers, 2024, pp. 295–352.
4 F. Z. Stanczyk, J. P. Hapgood, S. Winer and D. R. Mishell Jr, Progestogens used in postmenopausal hormone therapy: differences in their pharmacological properties, intracellular actions, and clinical effects, *Endocr. Rev.*, 2013, **34**, 171–208.
5 A. Roheel, A. Khan, F. Anwar, Z. Akbar, M. F. Akhtar, M. Imran Khan, M. F. Sohail and R. Ahmad, Global epidemiology of breast cancer based on risk factors: a systematic review, *Front. Oncol.*, 2023, **13**, 1240098.
6 M. S. Islam, S. Afrin, S. I. Jones and J. Segars, Selective progesterone receptor modulators—mechanisms and therapeutic utility, *Endocr. Rev.*, 2020, **41**, bnaa012.
7 J. D. Graham and C. L. Clarke, Physiological action of progesterone in target tissues, *Endocr. Rev.*, 1997, **18**, 502–519.
8 S. Zhao, Q. Gao, C. Rong, S. Wang, Z. Zhao, Y. Liu and J. Xu, Immunomodulatory effects of edible and medicinal mushrooms and their bioactive immunoregulatory products, *J. Fungi*, 2020, **6**, 269.
9 I. J. Suarez-Arroyo, R. Rosario-Acevedo, A. Aguilar-Perez, P. L. Clemente, L. A. Cubano, J. Serrano, R. J. Schneider and M. M. Martínez-Montemayor, Anti-tumor effects of Ganoderma lucidum (reishi) in inflammatory breast cancer in in vivo and in vitro models, *PLoS One*, 2013, **8**, e57431, DOI: 10.1371/journal.pone.0057431.
10 B. Boh, M. Berovic, J. Zhang and L. Zhi-Bin, Ganoderma lucidum and its pharmaceutically active compounds, *Biotechnol. Annu. Rev.*, 2007, **13**, 265–301.
11 F. Kou, Y. Ge, W. Wang, Y. Mei, L. Cao, X. Wei, H. Xiao and X. Wu, A review of Ganoderma lucidum polysaccharides: Health benefit, structure–activity relationship, modification, and nanoparticle encapsulation, *Int. J. Biol. Macromol.*, 2023, **243**, 125199.
12 S. Patel and A. Goyal, Recent developments in mushrooms as anti-cancer therapeutics: a review, *3 Biotech*, 2012, **2**, 1–15.
13 S. A. Noorian, N. Hemmatinejad and J. A. R. Navarro, Bioactive molecule encapsulation on metal-organic framework via simple mechanochemical method for controlled topical drug delivery systems, *Microporous Mesoporous Mater.*, 2020, **302**, 110199.
14 A. K. Aman, R. K. Singh, R. Kumar and A. K. Ghosh, Effect of high energy ball milling grinding on physico-chemical, morphological and optical properties of Curcuma longa nanoparticles powders, *Int. J. Pharm. Sci. Res.*, 2018, **9**, 672–677.

15 E. Juarez-Arellano, M. Urzua-Valenzuela, M. Peña-Rico, A. Aparicio-Saguilán, M. Valera-Zaragoza, A. Huerta and A. K. Navarro-Mtz, Planetary ball-mill as a versatile tool to controlled potato starch modification to broaden its industrial applications, *Food Res. Int.*, 2020, **140**, 109870, DOI: 10.1016/j.foodres.2020.109870.

16 J. M. Caster, K. Y. Stephanie, A. N. Patel, N. J. Newman, Z. J. Lee, S. B. Warner, K. T. Wagner, K. C. Roche, X. Tian and Y. Min, Effect of particle size on the biodistribution, toxicity, and efficacy of drug-loaded polymeric nanoparticles in chemoradiotherapy, *Nanomedicine*, 2017, **13**, 1673–1683.

17 C. Madusanka, D. Udayanga, R. Nilmini, S. Rajapaksha, C. Hewawasam, D. Manamgoda and J. Vasco-Correa, A review of recent advances in fungal mycelium based composites, *Discover Mater.*, 2024, **4**, 13.

18 M. E. Antinori, M. Contardi, G. Suarato, A. Armirotti, R. Bertorelli, G. Mancini, D. Debellis and A. Athanassiou, Advanced mycelium materials as potential self-growing biomedical scaffolds, *Sci. Rep.*, 2021, **11**, 12630.

19 A. Ubeyitogullari, S. Ahmadzadeh, G. Kandhola and J. Kim, Polysaccharide-based porous biopolymers for enhanced bioaccessibility and bioavailability of bioactive food compounds: Challenges, advances, and opportunities, *Compr. Rev. Food Sci. Food Saf.*, 2022, **21**, 4610–4639.

20 A. Qiu, Y. Wang, G. Zhang and H. Wang, Natural polysaccharide-based nanodrug delivery systems for treatment of diabetes, *Polymers*, 2022, **14**, 3217.

21 D. F. Roa, M. P. Buera, M. P. Tolaba and P. R. Santagapita, Encapsulation and stabilization of β-carotene in amaranth matrices obtained by dry and wet assisted ball milling, *Food Bioprocess Technol.*, 2017, **10**, 512–521.

22 S. P. Wasser, Medicinal mushrooms in human clinical studies. Part I. Anticancer, oncoimmunological, and immunomodulatory activities: a review, *Int. J. Med. Mushrooms*, 2017, **19**(4), 279–317.

23 V. Pucci, F. Bugamelli, R. Mandrioli, B. Luppi and M. A. Raggi, Determination of progesterone in commercial formulations and in non conventional micellar systems, *J. Pharm. Biomed. Anal.*, 2003, **30**, 1549–1559, DOI: 10.1016/S0731-7085(02)00547-2.

24 H. Khayam-Bashi and M. Boroumand, Spectrophotometric estimation of estradiol-17β, progesterone, and testosterone, *Biochem. Med.*, 1975, **14**, 104–108, DOI: 10.1016/0006-2944(75)90024-1.

25 O. Trott and A. J. Olson, AutoDock Vina: improving the speed and accuracy of docking with a new scoring function, efficient optimization, and multithreading, *J. Comput. Chem.*, 2010, **31**, 455–461.

26 D. S. Biovia, *BIOVIA Discovery Studio*, Dassault Systèmes, 2020.

27 N. Dharmasiri, S. Dharmasiri and M. Estelle, The F-box protein TIR1 is an auxin receptor, *Nature*, 2005, **435**, 441–445.

28 K. Yakin, F. Hela and O. Oktem, Progesterone signaling in the regulation of luteal steroidogenesis, *Mol. Hum. Reprod.*, 2023, **29**(8), gaad022.

29 D. A. Fruman, H. Chiu, B. D. Hopkins, S. Bagrodia, L. C. Cantley and R. T. Abraham, The PI3K pathway in human disease, *Cell*, 2017, **170**, 605–635.

30 C. H. Diep, A. R. Daniel, L. J. Mauro, T. P. Knutson and C. A. Lange, Progesterone action in breast, uterine, and ovarian cancers, *J. Mol. Endocrinol.*, 2015, **54**, R31–R53.

31 Y. Xu, P. Huangyang, Y. Wang, L. Xue, E. Devericks, H. G. Nguyen, X. Yu, J. A. Oses-Prieto, A. L. Burlingame and S. Miglani, ERα is an RNA-binding protein sustaining tumor cell survival and drug resistance, *Cell*, 2021, **184**, 5215–5229.

32 R. R. M. Paterson, Ganoderma–a therapeutic fungal biofactory, *Phytochemistry*, 2006, **67**, 1985–2001.

33 S. Wachtel-Galor, J. Yuen, J. A. Buswell and I. F. F. Benzie, *Ganoderma Lucidum (Lingzhi or Reishi): a Medicinal Mushroom*, 2012.

34 Y. Yang, H. Zhou, W. Liu, J. Wu, X. Yue, J. Wang, L. Quan, H. Liu, L. Guo and Z. Wang, Ganoderic acid A exerts antitumor activity against MDA-MB-231 human breast cancer cells by inhibiting the Janus kinase 2/signal transducer and activator of transcription 3 signaling pathway, *Oncol. Lett.*, 2018, **16**, 6515–6521.

35 Y.-L. Wu, F. Han, S.-S. Luan, R. Ai, P. Zhang, H. Li and L.-X. Chen, Triterpenoids from Ganoderma lucidum and their potential anti-inflammatory effects, *J. Agric. Food Chem.*, 2019, **67**, 5147–5158.

36 J. Zhao, Y. Fan, H. Li, C. Wang, S. Fan, H. Sun and M. Liu, Ganoderic Acid A Prevented Osteoporosis by Modulating the PIK3CA/p-Akt/TWIST1 Signaling Pathway, *Food Sci. Nutr.*, 2025, **13**, e70177.

37 P. Dey, R. P. A. Barros, M. Warner, A. Ström and J.-Å. Gustafsson, Insight into the mechanisms of action of estrogen receptor β in the breast, prostate, colon, and CNS, *J. Mol. Endocrinol.*, 2013, **51**, T61–T74.

38 J. Yang, J. Nie, X. Ma, Y. Wei, Y. Peng and X. Wei, Targeting PI3K in cancer: mechanisms and advances in clinical trials, *Mol. Cancer*, 2019, **18**, 26.

39 S. S. Singh, W. N. Yap, F. Arfuso, S. Kar, C. Wang, W. Cai, A. M. Dharmarajan, G. Sethi and A. P. Kumar, Targeting the PI3K/Akt signaling pathway in gastric carcinoma: A reality for personalized medicine?, *World J. Gastroenterol.*, 2015, **21**, 12261.

40 G. M. Morris, R. Huey, W. Lindstrom, M. F. Sanner, R. K. Belew, D. S. Goodsell and A. J. Olson, AutoDock4 and AutoDockTools4: Automated docking with selective receptor flexibility, *J. Comput. Chem.*, 2009, **30**, 2785–2791.

41 P. Vos, G. Garrity, D. Jones, N. R. Krieg, W. Ludwig, F. A. Rainey, K.-H. Schleifer and W. B. Whitman, *Bergey's Manual of Systematic Bacteriology: Volume 3: the Firmicutes*, Springer Science & Business Media, 2011.

42 Clinical and Laboratory Standards Institute (CLSI), M07: Clinical and Laboratory Standards Institute Methods for Dilution Antimicrobial Susceptibility Tests for Bacteria That Grow Aerobically, *Clin. Lab. Stand. Inst.*, 2018, 91.

43 P. Parvekar, J. Palaskar, S. Metgud, R. Maria and S. Dutta, The minimum inhibitory concentration (MIC) and minimum bactericidal concentration (MBC) of silver

nanoparticles against Staphylococcus aureus, *Biomater. Invest. Dent.*, 2020, **7**, 105–109.
44 M. Elshikh, S. Ahmed, S. Funston, P. Dunlop, M. McGaw, R. Marchant and I. M. Banat, Resazurin-based 96-well plate microdilution method for the determination of minimum inhibitory concentration of biosurfactants, *Biotechnol. Lett.*, 2016, **38**, 1015–1019.
45 U.S. FDA, *ICH Q1A (R2): Stability Testing of New Drug Substances and Products*, FDA, MD, USA, 2003.
46 O. González-González, I. O. Ramirez, B. I. Ramirez, P. O'Connell, M. P. Ballesteros, J. J. Torrado and D. R. Serrano, Drug stability: ICH versus accelerated predictive stability studies, *Pharmaceutics*, 2022, **14**, 2324.
47 K. C. Waterman and R. C. Adami, Accelerated aging: prediction of chemical stability of pharmaceuticals, *Int. J. Pharm.*, 2005, **293**, 101–125.
48 M. Blessy, R. D. Patel, P. N. Prajapati and Y. K. Agrawal, Development of forced degradation and stability indicating studies of drugs—A review, *J. Pharm. Anal.*, 2014, **4**, 159–165.
49 K. Huynh-Ba, *Handbook of Stability Testing in Pharmaceutical Development: Regulations, Methodologies, and Best Practices*, Springer, 2009.
50 M. Stevanović and N. Filipović, A review of recent developments in biopolymer nano-based drug delivery systems with antioxidative properties: Insights into the last five years, *Pharmaceutics*, 2024, **16**, 670.
51 O. Taofiq, S. A. Heleno, R. C. Calhelha, I. P. Fernandes, M. J. Alves, L. Barros, A. M. González-Paramás, I. C. F. R. Ferreira and M. F. Barreiro, Mushroom-based cosmeceutical ingredients: Microencapsulation and in vitro release profile, *Ind. Crops Prod.*, 2018, **124**, 44–52.
52 P. J. Palermo, Solid dosage-form analysis, in *Sep. Sci. Technol.*, Elsevier, 2001, pp. 235–267.
53 R. Shah, D. Eldridge, E. Palombo and I. Harding, Optimisation and stability assessment of solid lipid nanoparticles using particle size and zeta potential, *J. Phys. Sci.*, 2014, **25**(1), 59–75.
54 S. Dash, P. N. Murthy, L. Nath and P. Chowdhury, Kinetic modeling on drug release from controlled drug delivery systems, *Acta Pol. Pharm.*, 2010, **67**, 217–223.
55 P. J. Bums, J. V Steiner, P. L. Sertich, M. A. Pozor, T. R. Tice, D. W. Mason and D. F. Love, Evaluation of biodegradable microspheres for the controlled release of progesterone and estradiol in an ovulation control program for cycling mares, *J. Equine Vet. Sci.*, 1993, **13**, 521–524.
56 M. P. Weinstein and J. S. Lewis, The clinical and laboratory standards institute subcommittee on Antimicrobial susceptibility testing: Background, organization, functions, and processes, 2020, DOI: **10.1128/JCM.01864-19**.
57 A. Kamra and A. B. Bhatt, Evaluation of antimicrobial and antioxidant activity of Ganoderma lucidum extracts against human pathogenic bacteria, *Int. J. Pharm. Pharm. Sci.*, 2012, **4**, 359–362.
58 L. Qian, C. Chen, Y. Lv, J. Li, X. Cao, H. Ren and M. L. Hassan, Preparation and electrochemical application of porous carbon materials derived from extraction residue of Ganoderma lucidum, *Biomass Bioenergy*, 2022, **166**, 106593.
59 C. Sriket, S. Kuimalee, S. Yarnpakdee, S. Benjakul, P. Sriket, H. Kishimura, T. Senphan and S. Nalinanon, Elucidating the physicochemical and structural properties of Ganoderma lucidum spores: Comparative analysis of various disruption techniques, *Powder Technol.*, 2024, **439**, 119731.
60 J. Grgić, G. Šelo, M. Planinić, M. Tišma and A. Bucić-Kojić, Role of the encapsulation in bioavailability of phenolic compounds, *Antioxidants*, 2020, **9**, 923.
61 H. Rostamabadi, S. R. Falsafi, M. M. Rostamabadi, E. Assadpour and S. M. Jafari, Electrospraying as a novel process for the synthesis of particles/nanoparticles loaded with poorly water-soluble bioactive molecules, *Adv. Colloid Interface Sci.*, 2021, **290**, 102384.
62 Y. Liu, W. Lan, Y. Wang, W. Bai, H. Zhou and P. Wan, Differential analysis of Korean and Chinese Lingzhi or Reishi medicinal mushroom Ganoderma lucidum (Agaricomycetes) spore powder by infrared spectroscopy with stoichiometry, *Int. J. Med. Mushrooms*, 2023, **25**, 87–98.
63 B. Sangeetha, A. S. Krishnamoorthy, D. Amirtham, D. J. S. Sharmila, P. Renukadevi and V. G. Malathi, FT-IR spectroscopic characteristics of Ganoderma lucidum secondary metabolites, *J. Appl. Sci. Technol.*, 2019, **38**, 1–8.
64 S. P. Ospina Álvarez, D. A. Ramírez Cadavid, D. M. Escobar Sierra, C. P. Ossa Orozco, D. F. Rojas Vahos, P. Zapata Ocampo and L. Atehortúa, Comparison of extraction methods of chitin from Ganoderma lucidum mushroom obtained in submerged culture, *Biomed. Res. Int.*, 2014, **2014**, 169071.
65 S. M. Mousavi, S. A. Hashemi, A. Gholami, N. Omidifar, W.-H. Chiang, V. R. Neralla, K. Yousefi and M. Shokripour, Ganoderma lucidum methanolic extract as a potent phytoconstituent: characterization, in-vitro antimicrobial and cytotoxic activity, *Sci. Rep.*, 2023, **13**, 17326.
66 M. Fathi, M. Alami-Milani, M. H. Geranmayeh, J. Barar, H. Erfan-Niya and Y. Omidi, Dual thermo-and pH-sensitive injectable hydrogels of chitosan/(poly (N-isopropylacrylamide-co-itaconic acid)) for doxorubicin delivery in breast cancer, *Int. J. Biol. Macromol.*, 2019, **128**, 957–964.
67 S. Venkateswarlu, B. Viswanath, A. S. Reddy and M. Yoon, Fungus-derived photoluminescent carbon nanodots for ultrasensitive detection of Hg2+ ions and photoinduced bactericidal activity, *Sens. Actuators, B*, 2018, **258**, 172–183.
68 J. Xu, X. Jie, F. Xie, H. Yang, W. Wei and Z. Xia, Flavonoid moiety-incorporated carbon dots for ultrasensitive and highly selective fluorescence detection and removal of Pb 2+, *Nano Res.*, 2018, **11**, 3648–3657.
69 W.-J. Wang, J.-M. Xia, J. Feng, M.-Q. He, M.-L. Chen and J.-H. Wang, Green preparation of carbon dots for intracellular pH sensing and multicolor live cell imaging, *J. Mater. Chem. B*, 2016, **4**, 7130–7137.

70 T. Pal, S. Mohiyuddin and G. Packirisamy, Facile and green synthesis of multicolor fluorescence carbon dots from curcumin: in vitro and in vivo bioimaging and other applications, *ACS Omega*, 2018, **3**, 831–843.
71 R. Souza da Costa, W. Ferreira da Cunha, N. Simenremis Pereira and A. Marti Ceschin, An alternative route to obtain carbon quantum dots from photoluminescent materials in peat, *Materials*, 2018, **11**, 1492.
72 V. N. Mehta, S. Jha, R. K. Singhal and S. K. Kailasa, Preparation of multicolor emitting carbon dots for HeLa cell imaging, *New J. Chem.*, 2014, **38**, 6152–6160.
73 F. V. Leimann, M. H. Biz, K. C. Kaufmann, W. J. Maia, O. H. Honçalves, L. Cardozo Filho, C. Sayer and P. H. H. de Araújo, Characterization of progesterone loaded biodegradable blend polymeric nanoparticles, *Cienc. Rural*, 2015, **45**, 2082–2088.
74 G. Lv, Z. Zhang, H. Pan and L. Fan, Effect of physical modification of mushroom (A. chaxingu) powders on their physical and chemical properties, *Food Sci. Technol. Res.*, 2014, **20**, 731–738.
75 G. N. Mendes, L. G. Floresta, W. M. Takeshita, B. F. Brasileiro and C. L. Trento, The Application of ImageJ Software for Roughness Analysis of Dental Implants, *J. Imaging Inform. Med.*, 2024, 1–8.
76 V. Balamuralidhara, T. M. Pramodkumar, N. Srujana, M. P. Venkatesh, N. V. Gupta, K. L. Krishna and H. V Gangadharappa, pH sensitive drug delivery systems: a review, *Am. J. Drug Discovery Dev.*, 2011, **1**, 24–48.
77 I. S. Bayer, Controlled drug release from nanoengineered polysaccharides, *Pharmaceutics*, 2023, **15**, 1364.
78 U.S.P.C.C. of Experts, Simulated gastric fluid and simulated intestinal fluid, TS, United States Pharmacopeia, *Natl. Formul.*, 1995, **23**, 2207–2235.
79 X. Li and B. R. Jasti, *Design of Controlled Release Drug Delivery Systems*, McGraw-Hill Education, United Kingdom, 2006.
80 C. Carvalho, R. X. Santos, S. Cardoso, S. Correia, P. J. Oliveira, M. S. Santos and P. I. Moreira, Doxorubicin: the good, the bad and the ugly effect, *Curr. Med. Chem.*, 2009, **16**, 3267–3285.
81 U. Hafeez, S. Parakh, H. K. Gan and A. M. Scott, Antibody–drug conjugates for cancer therapy, *Molecules*, 2020, **25**, 4764.
82 M. C. Wani, H. L. Taylor, M. E. Wall, P. Coggon and A. T. McPhail, Plant antitumor agents. VI. Isolation and structure of taxol, a novel antileukemic and antitumor agent from Taxus brevifolia, *J. Am. Chem. Soc.*, 1971, **93**, 2325–2327.
83 S. Pushpa Ragini, A. V. Naga Divya and K. Y. V. Anusha, Enhancement of paclitaxel and doxorubicin cytotoxicity in breast cancer cell lines in combination with piperine treatment and analysis of expression of autophagy and apoptosis genes, *J. Med. Sci. Res.*, 2014, **2**, 62–67, DOI: **10.17727/jmsr.2014/2-012**.
84 F. Kalaycı-Yüksek, D. Gümüş, M. Anğ-Küçüker and F. Kalayci-Yüksek, Hormones can influence antibiotic susceptibilities even in mono-and co-culture conditions, *Acta Biol. Marisiensis*, 2021, **4**, 39–49.
85 A. Doğan, S. Otlu, Ö. Çelebi, P. Aksu, A. G. Sağlam, A. Doğan and N. Mutlu, An investigation of antibacterial effects of steroids, *Turk. J. Vet. Anim. Sci.*, 2017, **41**, 302–305.
86 G. Grover and S. G. Kini, Synthesis and evaluation of new quinazolone derivatives of nalidixic acid as potential antibacterial and antifungal agents, *Eur. J. Med. Chem.*, 2006, **41**, 256–262.
87 K. Waisser, J. Matyk, H. Divišová, P. Husakova, J. Kuneš, V. Klimešová, K. Palat and J. Kaustova, The Oriented Development of Antituberculotics (Part II): Halogenated 3-(4-Alkylphenyl)-1, 3-benzoxazine-2, 4-(3H)-diones, *Arch. Pharm.*, 2007, **340**, 264–267.
88 H. H. Ibraheem, Synthesis and Microbiological Investigation of Progesterone Derivatives, *Eng. Technol. J.*, 2013, **31**, 687–697.
89 T. Gürgan, B. Urman, K. S. Diker, L. Delilbasi and H. A. Kisnisci, Human follicular fluid from pre-ovulatory follicles in patients undergoing in-vitro fertilization inhibits the in-vitro growth of gram-positive micro-organisms, *Hum. Reprod.*, 1993, **8**, 508–510.
90 K. M. A. Daruliza, L. Fernandez, R. Jegathambigai and S. Sasidharan, Anti-Candida activity and brine shrimp toxicity assay of Ganoderma boninense, *Eur. Rev. Med. Pharmacol. Sci.*, 2012, **16**, 43–48.
91 D. N. Roy, A. K. Azad, F. Sultana and A. S. M. Anisuzzaman, In-vitro antimicrobial activity of ethyl acetate extract of two common edible mushrooms, *J. Phytopharm.*, 2016, **5**, 79–82.
92 P. Shah, H. A. Modi, M. D. Shukla and S. K. Lahiri, Preliminary phytochemical analysis and antibacterial activity of Ganoderma lucidum collected from Dang District of Gujarat, India, *Int. J. Curr. Microbiol. Appl. Sci.*, 2014, **3**, 246–255.
93 K. F. Farouk, N. Tahar, T. M. Esseddik, R. Redouane, B. Chawki, A. Pablo and P. Massimiliano, Antioxidant Activity and Phenolic Content of Wild Algerian Lingzhi or Reishi Medicinal Mushroom Ganoderma lucidum (Agaricomycetes) Extracts, *Int. J. Med. Mushrooms*, 2021, **23**(6), 79–88.
94 E. H. Erbiai, B. Amina, A. Kaoutar, R. Saidi, Z. Lamrani, E. Pinto, J. C. G. Esteves da Silva, A. Maouni and L. Pinto da Silva, Chemical characterization and evaluation of antimicrobial properties of the wild medicinal mushroom ganoderma lucidum growing in northern Moroccan forests, *Life*, 2023, **13**, 1217.
95 P. N. Waithaka, E. M. Gathuru, B. M. Githaiga and K. M. Onkoba, Antimicrobial Activity of Mushroom (Agaricus Bisporus) and Fungi (Trametes Gibbosa) Extracts from Mushrooms and Fungi of Egerton Main Campus, Njoro Kenya, in *5th KyU International Conference*, 2022.
96 E. Sande, D. L. Baraza, S. Ooko and P. K. Nyongesa, Isolation, characterization and antibacterial activity of ergosta-5, 7, 22-triene-3β, 14α–Diol (22Z) from Kenyan ganoderma lucidum, *Asian J. Appl. Chem. Res*, 2020, **5**, 48–57.

97 S. A. Heleno, I. C. F. R. Ferreira, A. P. Esteves, A. Ćirić, J. Glamočlija, A. Martins, M. Soković and M. J. R. P. Queiroz, Antimicrobial and demelanizing activity of Ganoderma lucidum extract, p-hydroxybenzoic and cinnamic acids and their synthetic acetylated glucuronide methyl esters, *Food Chem. Toxicol.*, 2013, **58**, 95–100.

98 H. Wang and T. B. Ng, Ganodermin, an antifungal protein from fruiting bodies of the medicinal mushroom Ganoderma lucidum, *Peptides*, 2006, **27**, 27–30.

99 Y. Meng, C. Qiu, X. Li, D. J. McClements, S. Sang, A. Jiao and Z. Jin, Polysaccharide-based nano-delivery systems for encapsulation, delivery, and pH-responsive release of bioactive ingredients, *Crit. Rev. Food Sci. Nutr.*, 2024, **64**, 187–201.

100 P. M. Junaid, A. H. Dar, K. K. Dash, S. Rohilla, R. Islam, R. Shams, V. K. Pandey, S. Srivastava, P. S. Panesar and S. Zaidi, Polysaccharide-based hydrogels for microencapsulation of bioactive compounds: A review, *J. Agric. Food Res.*, 2024, **15**, 101038.

101 S. Wasser, Medicinal mushroom science: Current perspectives, advances, evidences, and challenges, *Biomed. J.*, 2014, **37**, 345–356.

102 A. Sood, A. Gupta and G. Agrawal, Recent advances in polysaccharides based biomaterials for drug delivery and tissue engineering applications, *Carbohydr. Polym. Technol. Appl.*, 2021, **2**, 100067.

103 G. A. Pankey and L. D. Sabath, Clinical relevance of bacteriostatic versus bactericidal mechanisms of action in the treatment of Gram-positive bacterial infections, *Clin. Infect. Dis.*, 2004, **38**, 864–870.

104 Y. Kan, T. Chen, Y. Wu and J. Wu, Antioxidant activity of polysaccharide extracted from Ganoderma lucidum using response surface methodology, *Int. J. Biol. Macromol.*, 2015, **72**, 151–157.